Wormlike Chain Polymers Under External Fields with Applications to Nanotechnology

by

Nigel Thor Stanley Morgan Andersen

A thesis

presented to the University of Waterloo

in fulfillment of the

thesis requirement for the degree of

Master of Science

in

Physics

Waterloo, Ontario, Canada, 2022

Author's Declaration

This thesis consists of material all of which I authored or co-authored: see Statement of Contributions included in the thesis. This is a true copy of the thesis, including any required final revisions, as accepted by my examiners.

I understand that my thesis may be made electronically available to the public.

Statement of Contributions

This thesis contains content that was published, as well as content that is being prepared for publication. The content in chapter 2 and appendix B was published in Macromolecules in 2021 [1]. The content was co-authored with Yue Teng and Jeff Z.Y. Chen. It was reprinted (adapted) with permission from Andersen, N. T.; Teng, Y.; Chen, J. Z. Y. Stretching a Semiflexible Polymer of Finite Length. Macromolecules 2022, 55, 210-216. Copyright 2022 American Chemical Society. Chapter 3 is being prepared for publication, and its contents was co-authored with Jeff Z.Y. Chen. In both these cases, I was the majority author of the works, contributing heavily to the theory, and performing all of the numerical calculations. The majority of each manuscript was written by myself, with edits and contributions by my co-authors. Chapters 1 and 4, as well as appendix A and C, were sole-authored by myself.

Abstract

Polymers are long molecular chains formed from smaller molecular units called monomers. Polymers display interesting macroscopic properties, are ubiquitous in everyday materials, and are also important biomolecules among much else. The field of polymer science has been widely recognized for its contribution to using and understanding polymers in a wide range of applications. Here, using the common wormlike chain (WLC) polymer model, two systems are investigated. The first is polymer stretching. Finite length polymers are modelled under an external stretching field, and the resulting extension is analysed. The calculations are done numerically, as well as analytically when possible. Representative measures of the polymer conformations are computed using a novel perturbation theory, and the results are compared to other theories. Interpolation formulas are presented to summarize the theoretical findings. The second system is a single walled carbon nanotube, wrapped by a semiflexible polymer in a helical configuration. This type of spontaneous helical wrapping is widely studied experimentally due to its beneficial effects on nanotube solvation, with minimal effects on the underlying electronic properties of the nanotube. The WLC model is used to calculate the expected helix pitch, which is then compared against experimental observations. It is found to reproduce the results, as well as outperform the predictions of another competing model. The findings in both cases are summarized, and possible future research directions are discussed.

Acknowledgements

I wish to acknowledge my supervisor, Professor Jeff Z.Y. Chen, for supporting me throughout the development of this thesis.

Table of Contents

List of Figures

List of Tables

List of Abbreviations

- **BE** Backward Euler
- **DNA** Deoxyribonucleic Acid
- **FE** Forward Euler
- **FJC** Freely Jointed Chain
- **GC** Gaussian Chain
- **GSD** Ground State Dominance
- **KP** Kratky-Porod
- **MC** Monte Carlo
- **MD** Molecular Dynamics
- **MDE** Modified Diffusion Equation
- **PNES** poly[2,6-{1,5-bis(3-propoxysulfonicacidsodiumsalt)}naphthylene]ethynylene
- **PPES** poly[p-{2,5-bis(3-propoxysulfonicacidsodiumsalt)}phenylene]ethynylene
- **SWNT** Single Walled carbon Nanotube
- **WLC** Wormlike Chain
- **ssDNA** Single Stranded Deoxyribonucleic Acid

Chapter 1

Introduction

1.1 Background and Motivation

Brief Introduction to Polymer Science

Polymers are a unique class of molecules that are widespread both in modern technologies and materials, and fundamental to life in their important roles played as biomolecules in all organisms. The reader is no doubt familiar with many types of plastics and their uses, which are all composed of long polymer chains entangled with each other [26]. Long DNA polymers serve as the encoding material for genetic information in many organisms, humans included, while shorter liquid crystal polymers are the driving force behind many digital displays.

Since the 1950s, polymer physics has seen many important developments, and has had a large impact on both chemistry and physics. The impact of the field has been recognized through 7 Nobel Prizes, 6 in chemistry and one in physics. The first was awarded to Hermann Staudinger in 1953, who first contributed to the understanding of polymers as long chains of molecules linked together, breaking the common assumption that they were colloidal groupings of individual molecules [27]. It was followed up with the second Nobel Prize for chemistry in the field, jointly awarded to Julio Natta and Karl Ziegler for their work on the synthesis of these large molecules [28]. The first recognition of theoretical contributions was given to Paul J. Flory who was awarded the 1974 Prize in chemistry. Flory made several important developments to the field, for example, he introduced the concept of the theta temperature, at which the interactions of the polymer with itself are balanced out by the interactions between the polymer and the solvent, causing the polymer to behave as if it was in an ideal state; and important concept for understanding the behaviour of polymers in solution [29]. Following the work of Flory, the first Nobel Prize in physics for polymer science was awarded to Pierre-Gilles de Gennes in 1991. de Gennes made many contributions to both liquid crystals (semiflexible short molecules that can be described by the some of the same theory used for semi-

fliexible polymers discussed later), as well as the dynamics of polymers systems [30].

These works contributed much to the basis of the modern field of polymer science, in addition to the works of other authors such as Masao Doi, and Samuel F. Edwards who authored a classic textbook on the subject [31], and Theo Odijk, who made many classic contributions to scaling theories, among a host of other authors not mentioned here who made significant contributions to the field. The remaining Nobel Prizes in 2000 (Alan G. MacDiarmid, Alan J. Heeger, Hideki Shirakawa), 2002 (John Bennett Fenn, Koichi Tanaka, Kurt Wuthrich), and 2005 (Robert Grubbs, Richard Schrock, Yves Chauvin), recognized the expansion of the subject. The Prize in 2000 saw recognition for the development of electrically conductive polymer plastics with novel applications in electronics, and the 2002 Prize illustrated the important work done in analyzing biological macromolecules [32, 33]. The prize in 2005 furthered synthesis methods, paving the way for further advances in polymer types [34]. Of course, much work besides those recognized with a Nobel Prize has been carried out, with research in the field only continuing to grow, and further improvements and advances in both experimental and theoretical polymer physics are being made to this day.

Motivation

Polymers at their core are long molecules, composed of individual molecular units called monomers. The monomers themselves, how they bind together, and how many of them there are, determine the overall global properties of the polymer [35].

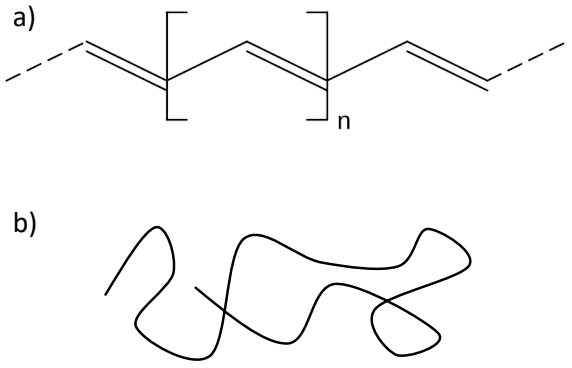

Figure 1.1: a) A sketch of the skeletal structure of *polyacetylene*, a basic polymer. The n th monomer is bracketed. b) A possible macroscopic configuration of polyacetylene, at large scales it behaves as a random curve, regardless of the microscopic structure.

Owing to the wide range of applications, there is a large body of both theoretical and experimental research on polymer systems. This includes both single chains and entangled polymer systems, in free space and confinement [31, 35]. In order to further development in the field, it is desirable to be able to explain experimentally studied systems using simple theories with a broad range of applications, as well as to improve upon older studies in areas where they are lacking.

This thesis takes a theoretical viewpoint on the subject. Theoretical methods in polymer science can be broken up into two general approaches, solving fundamental model, or simulating polymer systems using computers.

Within the realm of computer simulations, there are two common techniques: Monte Carlo (MC) simulations, and molecular dynamics (MD) simulations. MC simulations use random sampling to look for solutions of complex problems [36]. For example, one might obtain an accurate representation of the distribution function for a random walk polymer using MC methods by generating numerous random polymers and computing the statistics of the resulting samples. MD simulations approach the problem by modelling the interaction forces and potentials of the molecules, then simulating the evolution of the system using Newton's equations of motion, usually until an equilibrium state is achieved [37, 38]. One might construct the polymer of interest, model the interactions between the monomers making up the chain, and then evolve it in time to find an equilibrium configuration.

This thesis takes the other approach of solving a theoretical model and its associated equations. The basic model is the wormlike chain (WLC, see section 1.4), and the core technique is the Green's function method. The basic idea carried out is to construct a Hamiltonian described by the model, then construct a polymer by adding infinitesimal segments together, where the probability of adding each segment is described by a Boltzmann weight given by the Hamiltonian. Such a construction allows the formulation of a differential equation for the local distribution function (Green's function, see section 1.3.2 and 1.4). This local distribution function can be used to compute properties that depend on the average monomer positions, and it can also be used to compute the total partition function of the system. Once the total partition function is obtained, associated thermodynamic quantities of interest, such as the free energy, can be calculated from straightforward thermodynamic relations [39].

The current work aims apply this second approach to two problems, using the general WLC polymer theory. The first application is polymer stretching. The stretching of long double-stranded DNA was a seminal work in showing the applicability of the WLC model, by accurately reproducing experiments that stretched long DNA segments, which were not able to be reproduced using the simpler freely jointed chain (FJC, see section 1.3.1) [2]. However, there are many shorter polymers that can now be manipulated experimentally, and the theory developed only for long polymers, is in need of an update [40–45]. Following the basic WLC theory outlined in section 1.4, the problem of stretching a semiflexible polymer of finite length is covered in chapter 2.

The second problem is the helical wrapping of singled walled carbon nan-

otubes by long semiflexible polymers. The wrapping of carbon nanotubes by polymers is widely studied experimentally due to the ability of the polymers to solvate the nanotubes without affecting their electronic properties [46–51]. While molecular dynamics simulations have been carried out for individual experimental systems, no comprehensive study has been done using the WLC model [8–10, 13–15]. As is shown in chapter 3, use of the WLC model allows examination of the problem over a large parameter range, which in turn enables comparison against multiple experimental and theoretical systems.

1.2 Structure

This work is structured as follows. The remainder of the introduction contains the theoretical background that is required to understand the contributions in later chapters. Section 1.3 introduces some basic polymer models, and addresses their shortcomings. Section 1.4 discusses the WLC theory, the model used in the rest of this work, and notes how the relevant physical parameters are extracted from its framework. The numerical methods used to solve the general WLC theory in the absence of analytic solutions is given in section 1.5.

Chapter 2 discusses the stretching of semiflexible polymers using the WLC model. The background and motivations are introduced in detail. The extension of the general WLC to the stretching problem is shown, along with numerical and analytic results, and a comparison to other theories.

Modelling the helical wrapping of carbon nanotubes is discussed in chapter 3. Again, the extension of the general model to the carbon nanotube system is discussed. Numerical and closed form results are presented, and a full comparison to a range of experimental data as well as a competing theory is given.

Finally, chapter 4 provides a general summary of the results presented in this work. In addition, an outlook on possible further research is given, along with potential impacts.

1.3 A Simple Polymer Model

1.3.1 Freely Jointed Chain

The most basic polymer model is the Freely Jointed Chain (FJC). It assumes that the basic monomeric units can freely rotate around each other, meaning there is no energy cost for deforming the polymer, and the orientation of the bonds connecting the individual monomers together are uncorrelated [31]. Though there are no relations between monomers in the FJC, entropic considerations give rise to a finite polymer size in free space. Its size cannot be characterized by average end-to-end distance of the polymer $\langle \mathbf{R} \rangle$, because for such an isotropic distribution $\langle \mathbf{R} \rangle = 0$. Instead, a common measure of polymer size is the mean squared end-to-end distance $\langle \mathbf{R}^2 \rangle$, which has a finite value. For the FJC this can be simply calculated. Taking $\mathbf{r}_n$ as the bond vector for the

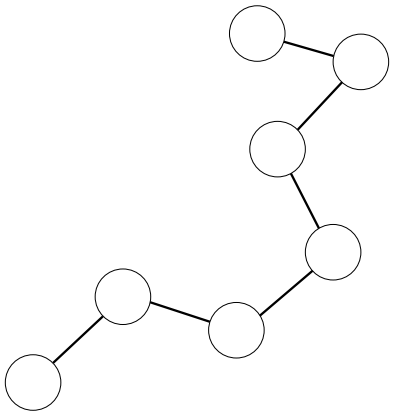

Figure 1.2: A schematic of a freely jointed chain (FJC) in 2D. The monomers are all separated by the same distance, and are oriented randomly with respect to each other, creating a random walk configuration.

n^{th} bond of a chain with N monomers [31]:

$$\langle \mathbf{R}^2 \rangle = \sum_{n,m}^{N} \langle \mathbf{r}_n \cdot \mathbf{r}_m \rangle = \sum_{n}^{N} \langle \mathbf{r}_n^2 \rangle + 2 \sum_{n>m} \langle \mathbf{r}_n \cdot \mathbf{r}_m \rangle \tag{1.1}$$

$$\langle \mathbf{R}^2 \rangle = N b_0^2 \tag{1.2}$$

where the second sum in (1.1) disappears because the bond vectors are uncorrelated. The bond length between two monomers b_0 has been introduced. When compared to the distribution of a real polymer, the FJC grossly underestimates $\langle \mathbf{R}^2 \rangle$, due to the bond vector correlations present in real polymers. However, the FJC can be made to match the distribution of undeformed polymer in solution through the introduction of an effective bond length b, known as the Kuhn length. The Kuhn length is the distance over which the correlations between the bond vectors in the real polymer have died out, and so monomers separated by this distance appear uncorrelated, and the polymer acts as a FJC with an effective monomer size b [35]. This gives

$$\langle \mathbf{R}^2 \rangle = N b^2 \tag{1.3}$$

or in terms of the total contour length of the polymer $L = Nb$,

$$\langle \mathbf{R}^2 \rangle = L b \tag{1.4}$$

1.3.2 Gaussian Chain

For the calculation of other statistical properties (and as a primer for later theory), it is useful to consider the continuous Gaussian chain (or simply Gaussian

chain) GC model. The discrete GC is a FJC where the bond lengths are taken to have a Gaussian distribution such that $\langle \mathbf{r}^2 \rangle = b_0^2$, and so it exhibits the same statistics as the FJC model. This is equivalent to having a harmonic potential between the bonds, and in the continuum limit allows the easy definition of the Hamiltonian for the GC as [31, 52].

$$\beta H_{\mathrm{GC}} = \int_0^1 \left[\frac{D}{2Lb} \left| \frac{\mathrm{d}\mathbf{r}(t)}{\mathrm{d}t} \right|^2 + U[\mathbf{r}(t)] \right] \mathrm{d}t \tag{1.5}$$

Here, the polymer has been parametrized using the arc variable t, where the polymer ends are specified by $t = 0$ and $t = 1$, and a polymer segment from $t = 0$ to $t = t'$ has a contour length Lt'. The spatial position of the polymer curve is given by $\mathbf{r}(t)$, and $U[\mathbf{r}(t)]$ is a reduced external potential that has spatial dependence. The factor of D is the dimensionality of the problem, and in free space is 3.

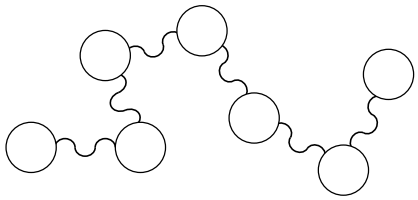

Figure 1.3: Schematic of a discrete Gaussian chain (GC). Harmonic springs connect the monomers, which are randomly oriented relative to one another. This results in each bond length, and hence the overall polymer end to end distance, having a Gaussian distribution.

Although statistically identical to the freely jointed chain model in terms of its free space distribution, this form has a distinct advantage over is discrete counterpart when it comes to computing elements of the distribution. We can in most cases, without a loss of generality, fix one end of the polymer at the origin $\mathbf{r}(0) = 0$. We can then introduce the Green's function, or propagator, $q(\mathbf{r}, t)$, which represents the partition function of all chain conformations with an end point at $\mathbf{r}(t)$. By constructing a polymer by considering infinitesimal additions governed by a Boltzmann weight $\exp(-\beta H_{\mathrm{GC}})$, one finds that the propagator satisfies a diffusion type differential equation

$$\frac{\partial}{\partial t} q_{\mathrm{GC}}(\mathbf{r}, t) = \left[\frac{Lb}{2D} \nabla_{\mathbf{r}}^2 - U(\mathbf{r}) \right] q_{\mathrm{GC}}(\mathbf{r}, \mathbf{t}) \tag{1.6}$$

The derivation of the above has been well documented elsewhere [31]. The use of the Green's function formalism provides several advantages. Since $q(\mathbf{r}, t)$ rep-

resents the partition function for a fixed end point, the total partition function of the chain is given by integrating the endpoint over volume of the system

$$Q_{\mathrm{GC}} = \int q_{\mathrm{GC}}(\mathbf{r}, t = 1)\,\mathrm{d}\mathbf{r} \tag{1.7}$$

hence the free energy and associated quantities of the system can be easily computed.

Physical properties dependent on the position of individual segments can be calculated using the monomer density distribution, obtained by integrating over all monomers along the chain the product of the partition functions for each segment on either side of the monomer of interest:

$$\rho_{\mathrm{GC}}(\mathbf{r}) = \frac{1}{Q_{\mathrm{GC}}} \int_0^1 q_{\mathrm{GC}}(\mathbf{r}, t) q_{\mathrm{GC}}(\mathbf{r}, 1 - t)\,\mathrm{d}t \tag{1.8}$$

The solving of equation (1.6) can either be done exactly, or numerically when an exact solution is not available. For details on different numerical methods that can be used, see section 1.5. The mean squared end-to-end distance for a free space polymer can easily be calculated under this formalism. The propagator solving equation 1.6 in 1D is the normalized Gaussian

$$q(x, t) = (2\pi Lbt)^{-1/2} e^{-x^2/2Lbt} \tag{1.9}$$

because there are no correlations between the bonds, the propagator for an n dimensional system is simply the product of n 1D propagators

$$q(\mathbf{r}, t) = (2\pi Lbt)^{-n/2} e^{-\mathbf{r}^2/2Lbt} \tag{1.10}$$

The mean squared end-to-end distance is then given by the second moment of the above distribution at $t = 1$ (the distribution function for the endpoints), which for a Gaussian can be read off of directly, giving

$$\langle R_{\mathrm{GC}}^2 \rangle = Lb \tag{1.11}$$

which as stated is the same for the FJC. In general, the GC model fails to properly capture the physics of the underlying polymer by not accounting for polymer stiffness, and instead the more advanced wormlike chain model, which takes into account the stiffness of the chain through the persistence length λ, must be used. It is worth noting however, that under certain conditions the GC model is valid, and may be readily applied to produce equivalent results to the wormlike chain model discussed in the next section. The conditions for equivalence are summarized in section 1.4.1.

1.4 Wormlike Chain Polymer Model

The wormlike chain (WLC) is a more advanced polymer model, that incorporates the polymer backbone stiffness through an energy cost for bending adjacent monomers, characterized through the persistence length λ. The persistence length is the characteristic distance over which the correlations between

tangent vectors along the chain die off. Specifically, for a free space chain with no external field and a energetic cost for bending two adjacent monomers ϵ, the correlations between the tangent vector at a point Lt along the chain, and the tangent vector at a point Lt' along the chain can be shown to be [53]

$$\langle \mathbf{u}(t) \cdot \mathbf{u}(t') \rangle = e^{-L|t'-t|/\lambda} \tag{1.12}$$

where the persistence length λ, the elastic bending constant ϵ divided by the Boltzmann constant times the temperature $\lambda = \epsilon/k_B T$, is the characteristic decay rate of the correlation function. The discrete WLC model was first proposed by Kratky and Porod, but here we focus on the continuous version best formulated by Saitô et al., which allows use of the Green's function formalism, and has a corresponding Hamiltonian [53, 54]

$$\beta H_{\mathrm{WLC}} = \int_0^1 \left[\frac{\lambda}{2L} \left| \frac{\mathrm{d}\mathbf{u}(t)}{\mathrm{d}t} \right|^2 + U[\mathbf{r}(t), \mathbf{u}(t)] \right] \mathrm{d}t \tag{1.13}$$

As before, L represents the total contour length of the polymer. The energy cost of bending is related to the tangent vector along the chain $\mathbf{u}(t) = \mathrm{d}\mathbf{r}(t)/\mathrm{d}t$. The reduced external potential $U[\mathbf{r}(t), \mathbf{u}(t)]$ can now have orientational dependence.

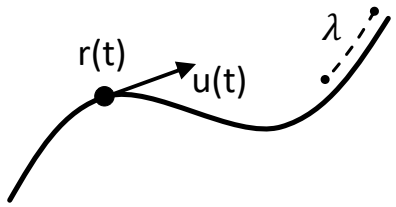

Figure 1.4: Schematic of a continuous wormlike chain (WLC), showing the position vector $\mathbf{r}(t)$, tangent vector $\mathbf{u}(t)$, and persistence length λ.

In the absence of any external field or confinement, the mean squared end-to-end distance of this model in 3D, called the Krakty-Porod mean squared end-to-end distance, is [54]

$$\langle \mathbf{R}^2_{\mathrm{KP/WLC}} \rangle = 2\lambda^2 \left[L/\lambda + e^{-L/\lambda} - 1 \right] \tag{1.14}$$

In the limit of a long / flexible chain $L/\lambda \gg 1$, the above reduces to the GC result

$$\langle \mathbf{R}^2_{\mathrm{WLC}} \rangle = \langle \mathbf{R}^2_{\mathrm{GC}} \rangle = 2\lambda L \tag{1.15}$$

where the Kuhn length is $b = 2\lambda$. In the rodlike limit, where the persistence length is much greater than the contour length $L\lambda \ll 1$, the mean squared end-to-end distance reduces to that of a freely rotating rod in free space

$$\langle \mathbf{R}^2_{\mathrm{WLC}} \rangle = L^2 \tag{1.16}$$

By following a similar derivation as for the Gaussian chain, under the Green's function formalism, one can show that the propagator $q(\mathbf{r}(t), \mathbf{u}(t), t)$ satisfies a similar modified diffusion equation [52, 53, 55]

$$\frac{\partial}{\partial t} q(\mathbf{r}, \mathbf{u}, t) = \left[-L\mathbf{u} \cdot \nabla_{\mathbf{r}}\big|_{\mathbf{u}} + \frac{L}{2\lambda} \nabla^2_{\mathbf{u}} - U[\mathbf{r}, \mathbf{u}] \right] q(\mathbf{r}, \mathbf{u}, t) \tag{1.17}$$

Here, the first term represents contributions from variations in the monomer density (e.g from confinement), and is inversely proportional to the size of the confinement. The second term is always present, and is due to the WLC bending. The third term is the reduced external potential as written in the Hamiltonian [52]. Once the propagator $q(\mathbf{r}, \mathbf{u}, t)$ is found, the partition function can be obtained through

$$Q_{\mathrm{WLC}} = \int q(\mathbf{r}, \mathbf{u}, t = 1) \, \mathrm{d}\mathbf{r}\mathrm{d}\mathbf{u} \tag{1.18}$$

and the density distribution can be obtained through

$$\rho(\mathbf{r}, \mathbf{u}) = \frac{1}{Q_{\mathrm{WLC}}} \int_0^1 q(\mathbf{r}, \mathbf{u}, t) q^*(\mathbf{r}, \mathbf{u}, t) \, \mathrm{d}t \tag{1.19}$$

Here $q(\mathbf{r}, \mathbf{u}, t)$ represents the partition function of the chain segment from $t = 0$ to $t = t'$, the complementary propagator $q^*(\mathbf{r}, \mathbf{u}, t)$ is the partition function from $t = t'$ to $t = 1$. As before their product links the two distributions on either side of the monomer of interest. The partition function Q_{WLC} and the density distribution $\rho(\mathbf{r}, \mathbf{u})$ together can be used to find most physical properties of interest.

The WLC model as presented under the Green's function formalism is a fundamental model that is widely used in polymer physics. It not only captures the undeformed free space statistics as does the Gaussian chain, but also accurately reproduces experiments where polymers are strongly deformed, such as stretching [2]. In many specific cases, solutions to equation (1.17) can be determined through careful analysis. However, in general, a full solution must be obtained numerically. Fortunately, numerical solutions for these types of equations are well studied, and several common methods are discussed later in section 1.5.

1.4.1 Reduction to the Gaussian Chain

In general, the WLC model is required to properly capture the physics of the underlying polymer. However, under several limits, the WLC model reduces to the GC model. The three conditions for equivalence are [52]

1. Long chain / Flexible. The contour length of the polymer needs to be much larger than the persistence length, $L/\lambda \gg 1$.

2. Weak variation. The typical length scale over which the system varies is of the order $\sqrt{Lb}$ or larger.

3. Weak external field. The reduced external potential U must be of order $(b/L)^0 = 1$ or smaller.

If all three conditions are satisfied, then it is valid to use the GC model in place of the WLC. They insure the system is being probed entropically, and so the underlying structure of the polymer has little effect on the statistics. If any one of them is not satisfied, then the full WLC model must be used. For the systems dealt with in the later chapters, the strong external potential breaks condition 3, and hence use of the WLC is paramount.

1.5 Numerical Methods

This section covers the general idea of numerical solutions to partial differential equations, in which the function domain is discretized into a finite set of points, and the equation of interest is solved numerically. Section 1.5.1 covers the very basics of the theory, while sections 1.5.2 and 1.5.3 cover the two simplest techniques, the forward and backward Euler methods. Section 1.5.4 discusses the Crank-Nicolson method, which is the numerical method used for the solutions in this work, and is based off of the two Euler methods. Finally, section 1.5.5 talks about Richardson extrapolation, which can be used to improve the scaling of the error with regard to grid size.

1.5.1 Numerical Integration

The basic idea behind numerical integration is to approximate the operators in a differential equation with a finite difference, allowing them to be treated numerically. Consider a 1D function $f(x)$, one can separate its domain into a grid with a uniform spacing Δx. There are then three basic ways to approximate the differential operator $\partial/\partial x$, either by considering the forward, backwards, or central differences of the function over the grid points [56].

$$\frac{\partial}{\partial x} = \frac{f(x+\Delta x) - f(x)}{\Delta x} \qquad \text{Forward difference} \qquad (1.20)$$

$$\frac{\partial}{\partial x} = \frac{f(x) - f(x-\Delta x)}{\Delta x} \qquad \text{Backwards difference} \qquad (1.21)$$

$$\frac{\partial}{\partial x} = \frac{f(x+\Delta x) - f(x-\Delta x)}{\Delta x} \qquad \text{Central difference} \qquad (1.22)$$

Similarly, by recursive application of the above, one can arrive at the approximation for second order derivatives

$$\frac{\partial^2}{\partial x^2} = \frac{f(x+2\Delta x) - 2f(x+\Delta x) + f(x)}{\Delta x^2} \qquad \text{Forward difference} \qquad (1.23)$$

$$\frac{\partial^2}{\partial x^2} = \frac{f(x) - 2f(x-\Delta x) + f(x-2\Delta x)}{\Delta x^2} \qquad \text{Backwards difference} \qquad (1.24)$$

$$\frac{\partial^2}{\partial x^2} = \frac{f(x+\Delta x) - 2f(x) + f(x-\Delta x)}{\Delta x^2} \qquad \text{Central difference} \qquad (1.25)$$

The choice of approximations defines the numerical method.

1.5.2 Forward Euler

The most basic method is the forward Euler method, which uses the forwards approximation of the derivative [56]. For the problems discussed in this work, the spatial derivative can always be best approximated by the central difference, and the choice of method only effects how the $\partial/\partial t$ derivative is handled. As an example, consider the free space 1D version of the general 3D WLC diffusion equation given in equation (1.17) with no external potential

$$\frac{\partial}{\partial t} q(x,t) = \left[\frac{L}{2\lambda}\frac{\partial^2}{\partial x^2}\right] q(x,t) \qquad (1.26)$$

By approximation the arc derivative along the contour with a forwards difference, and the spatial derivative with a second order central difference, then we arrive at the forward Euler method for this equation:

$$\frac{q(x,t+\Delta t) - q(x,t)}{\Delta t} = \left[\frac{L}{2\lambda}\left(\frac{q(x+\Delta x,t) - 2q(x,t) + q(x-\Delta x,t)}{\Delta x^2}\right)\right] \qquad (1.27)$$

Using the initial condition $q(x, t = 0) = 1$ and iterating using the above until $q(x, t = 1)$ is determined solves the equation. The error per step for this method is $\mathcal{O}(\Delta t) + \mathcal{O}(\Delta x^2)$, which can be determined by substituting the exact solution into the numerical scheme equation (1.27), then Taylor expanding and keeping the lowest order terms in both x and t. This method is fast, with reasonable accuracy, but can exhibit stability issues depending on Δt and Δx [57].

1.5.3 Backward Euler

The backward Euler method follows the same ideas as laid out in the discussion on the forward Euler method, but this time the derivative $\partial/\partial t$ is replaced with the backwards difference [56]. This results in

$$\frac{q(x,t+\Delta t) - q(x,t)}{\Delta t} = \left[\frac{L}{2\lambda}\left(\frac{q(x+\Delta x,t+\Delta t) - 2q(x,t+\Delta t) + q(x-\Delta x,t+\Delta t)}{\Delta x^2}\right)\right] \qquad (1.28)$$

This error scaling is, $\mathcal{O}(\Delta t) + \mathcal{O}(\Delta x^2)$, the same as the forward Euler method, but with the benefit of being stable for any Δt. The downside is that the numerical method is an implicit equation for $q(x, t + \Delta t)$ and so each step requires multiplication of $q(x, t)$ by an $n \times n$ solution matrix to the implicit scheme, where n is the number of grid points in x. The n^2 multiplication operations per step contributes to a significant increase in time compared to the $3n$ typically required for the forward Euler method. It is worth noting however, that the matrix inversion needs only to be done once with the inverted matrix reused for each time step, and hence only adds a (typically small) overhead to the method.

1.5.4 Crank-Nicolson

Crank-Nicolson is the numerical method that is used for all the calculations in this work that require full solutions of the WLC diffusion equation. If we denote the forward Euler method as $\mathrm{FE}(x, t)$ and the backward Euler method as $\mathrm{BE}(x, t)$, the Crank-Nicolson is given as the average of the two

$$\frac{q(x, t + \Delta t) - q(x, t)}{\Delta t} = \frac{1}{2}\big[\mathrm{FE}(x, t) + \mathrm{BE}(x, t)\big] \tag{1.29}$$

This inherits both the stability and the implicit nature of the backward Euler method, but with a better local truncation error of $\mathcal{O}(\Delta t^2)+\mathcal{O}(\Delta x^2)$. Although being an implicit scheme the method is inherently slower than the forward Euler method, it is by no means slow, and can reasonably be implemented on a personal computer for $\Delta t \approx 10^{-3}$ with a $10^3 \times 10^3$ matrix. If high accuracy is required, further computational techniques, such as the Richardson extrapolation discussed in the next section, can be used.

1.5.5 Richardson Extrapolation

In the cases when high accuracy is desired, it is beneficial to employ other numerical techniques instead of simply increasing the number of grid points in the numerical method. One of these methods is Richardson extrapolation. The basic principle is this [58]: the error E^h for a finite difference method typically goes as

$$E^h = C\Delta x^\nu + \mathcal{O}(\Delta x^{\nu+1}) \tag{1.30}$$

where C is some constant and ν is an integer. This is the case for all the methods discussed in this work. The differences between two approximations $U_1 - U^h$ and $U_0 - U^h$, if the U_1 approximation is generated with half the grid spacing compared to U_0, is

$$U_1 - U^h = \frac{1}{2^\nu}[U_0 - U^h] + \mathcal{O}(\Delta x^{\nu+1}) \tag{1.31}$$

which is obtained through equation 1.30. Rearranging the above for the numerical approximation U^h gives

$$U^h = \frac{2^\nu U_1 - U_0}{2^\nu - 1} + \mathcal{O}(\Delta x^{\nu+1}) \tag{1.32}$$

So by using two approximations U_0 and U_1 where the grid spacing of one is half that of the other, a third approximation U^h with an improved truncation error of $\mathcal{O}(\Delta x^{\nu+1})$ can be obtained. U^h is referred to as the Richardson extrapolation of U_0 and U_1 [58–60].

Although this requires the generation of two separate data sets, due to the improved error scaling it ends up being computationally more efficient than simply reducing the grid spacing until the desired error is achieved. In our case where the error depends both on the grid spacing of t, Δt, and that of x, Δx, applying Richardson extrapolation in both variables requires the generation of 4 unique data sets. However, even in this case it remains computationally efficient, and the data sets can be generated in parallel by leveraging distributed computational resources. For example, the data sets in 2 where generated using Compute Canada's Graham cluster, with caculations being complete in less than 24 hours, and using less than 10 GB of memory.

Chapter 2

Stretching Wormlike Chains of Finite Length

This chapter tackles the first major application of the wormlike chain (WLC) theory outlined in chapter 1. The WLC model is updated with an external potential corresponding to an applied force, and employed to the problem of polymer stretching. The theory presented then depends on two parameters, the stiffness and the external force. Adopting common theoretical and computational approaches, a high precision numerical solution is presented over a large range of the parameter space, with new analytic theories developed for certain limits. The validity of previous theoretical studies, and new analytic theories presented in this chapter, are analysed using the numerical solution as the benchmark. The contents of this chapter were published in Macromolecules in 2021 [1]

2.1 Introduction

Following several experimental studies, in 1995 Marko and Siggia presented a seminal paper capturing the physics behind the stretching of long polymers using the wormlike chain model [2, 31, 61–63]. The system is conceptually shown in Fig. 2.1(a). Analytic theories and approximate formulae have been presented to relate the polymer extension, $\langle z \rangle$, to the magnitude of the applied force, f, both in the original Marko and Siggia version and the later improved versions [3, 4]. The applicability of the above theoretical studies is limited to the case of long polymer, i.e., when the contour length of the polymer L is much greater than its persistence length λ. Many real systems, such as actin filaments, can have a finite L comparable to their λ. This has naturally prompted numerous theoretical and experimental studies on the force-extension properties of semiflexible polymers of finite length [5, 6, 40–45, 64–66].

The wormlike chain (WLC) model, as outlined in section 1.4, has been used as a theoretical tool for the description of polymer conformations. The forced

stretching problem adds to the original free-space model a potential energy term characterized by a prefactor f. For the finite-chain problem, previous theoretical studies featured Monte Carlo computer simulations (mostly based on the discrete version of the WLC) or analytical solutions to the partition function of the WLC Hamiltonian, for specific parameter regimes [40, 64, 67, 68]. Figure 2.1(b) shows the parameter space, described by $L/2\lambda$ and a reduced force. Considering the even simpler problem of a finite WLC without excluded volume, most studies have not provided a comprehensive view of the behaviour spanning from the known extension-force relations of rodlike filaments, through to the long polymer results originally presented by Marko and Siggia. The exceptions are the theoretical studies of Kierfeld et al. as well as Kessler and Rabin [5, 6]. As will be discussed below, a critical examination of their interpolation formulae against the high-precision numerical solution found in this work reveals inadequacy.

The goal of the current chapter is three-fold. First, to present a numerical solution to the standard WLC polymer model with the stretching potential, in order to provide comprehensive extension-force data covering the entire parameter space. The high precision data is presented for the crossover from rodlike to long-chain behaviour, as well as from weak to strong stretching behaviour, both as tabulated data, and as an interpolation formula. Second, to validate key analytic results in the three asymptotic regimes of weakly stretched, rodlike, and strongly stretched, which are assessed and clearly identified in the parameter space shown in Fig. 2.1(b). Finally, to calculate and analyse the mean square end-to-end distance of the stretched polymer projected on the plane perpendicular to the applied force. Both known and new analytic theories are presented and verified via numerical calculations, which are in turn all covered by a single interpolation formula. Together these three points allow an examination of previously unverified analytic results, while presenting both numerical and closed-form solutions for a regime that has not been generally addressed.

2.2 Free Space WLC with Stretching Force

We start with the ideal WLC model as discussed in section 1.4, where the general external potential becomes an external stretching force along the z direction $\mathbf{f} = f\hat{z}$. As before, the variable t ranges from 0 to 1, and parametrizes the curve representing the polymer. Because the system is in free space, there is no spatial dependence, and the Hamiltonian depends only on the tangent vector $\mathbf{u}(t) = \mathrm{d}\mathbf{r}(t)/\mathrm{d}t$. The stretched WLC is described by the reduced Hamiltonian [2, 31],

$$\beta H = \int_0^1 \left[\frac{\lambda}{2L} \left| \frac{\mathrm{d}\mathbf{u}(t)}{\mathrm{d}t} \right|^2 - \beta L f u_z(t) \right] \mathrm{d}t, \tag{2.1}$$

Here $u_z = \mathbf{u} \cdot \hat{z} = \cos\theta$ is the projection of the unit vector $\mathbf{u}$ on z. The ratio between the contour length L and the persistence length λ characterizes the relative flexibility of the chain. We refer to the limit $L/\lambda \gg 1$ as the flexible-chain

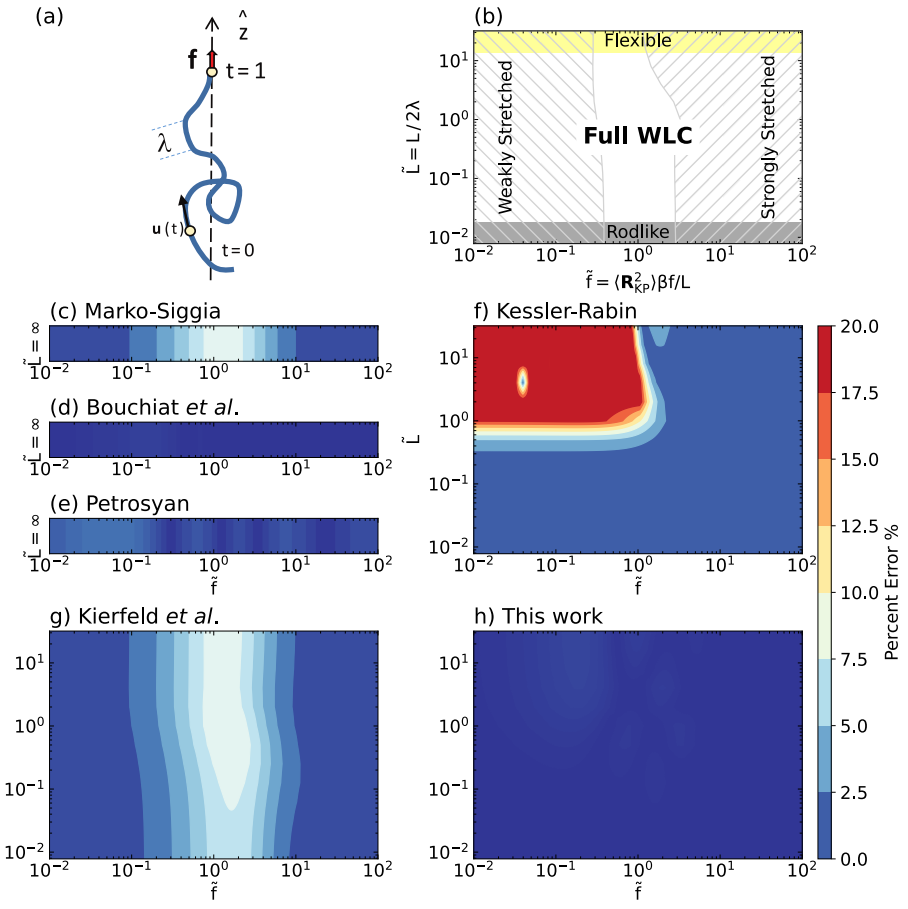

Figure 2.1: (a) Schematic of a stretched polymer of length L and persistence length λ, (b) the parameter regimes considered, (c)-(g) comparison of interpolation formulae (see Sect. 2.3.3) relating the force to the extension [2–6], against the numerical result. The new global interpolation formula presented here, Eq. (2.21), is used in (h), and has a maximum percent error of 1%. The shaded areas in (b) are discussed in the text. The reduced length $\tilde{L} \equiv L/2\lambda$ and force $\tilde{f} \equiv \langle \mathbf{R}^2_{\mathrm{KP}} \rangle \beta f / L$ are used as the system parameters.

limit, $L/\lambda \ll 1$ the rodlike limit, and a finite nonzero L/λ as a semiflexible chain having a finite length. The model has two reduced, dimensionless parameters,

$$\tilde{L} \equiv L/2\lambda \tag{2.2}$$

and $\beta L f$. Because in free space for long WLC the effective Kuhn length is 2λ, we scale L using 2λ as a basic unit.

The first goal is the extension between the two polymer ends, $\langle z \rangle$, which can be computed from

$$\frac{\langle z \rangle}{L} = \left\langle \int_0^1 u_z(t)\,\mathrm{d}t \right\rangle \equiv \langle \cos\theta \rangle = \frac{1}{\beta L}\frac{\partial \ln Q}{\partial f}, \tag{2.3}$$

through the standard thermodynamic relation for the Gibbs free energy, obtained through the partition function Q. The partition function itself is obtained using the propagator $q(\mathbf{u}, t)$, through

$$Q/V = \int q(\mathbf{u}, t=1)\,\mathrm{d}\mathbf{u} \tag{2.4}$$

In spherical coordinates, with θ being the angle from the z axis, and ϕ being the azimuthal angle, the stretched wormlike chain has rotational symmetry in ϕ and so the propagator reduces to have a dependence on θ only. The diffusion equation for the WLC in spherical coordinates under this symmetry can be shown to be [52]

$$\frac{\partial}{\partial t} q(\theta, t) = \left[\tilde{L} \left(\frac{1}{\sin\theta} \frac{\partial}{\partial \theta} \sin\theta \frac{\partial}{\partial \theta} \right) + \beta L f \cos\theta \right] q(\theta, t) \tag{2.5}$$

where the initial condition is still $q(\theta, 0) = 1$. While for this system, no general closed form solution exists, under certain limits exact solutions can be determined. These are discussed along with full numerical results in section 2.3.

2.3 Results

2.3.1 Analysis in Exact Limits

In three limits of the parameter space (rodlike, weakly stretched, strongly stretched) shown in Fig. 2.1(b), analytic expressions can be found for $\langle z \rangle / L$. No closed form eFor a rodlike polymer when $\tilde{L} \to 0$, one analytically obtains $q(\theta, t) = \exp(Lt\beta f \cos\theta)$ from (2.5), equivalent to a freely jointed chain with two monomers and a bond length L, which yields [35]

$$\frac{\langle z \rangle}{L} = \coth(\beta f L) - \frac{1}{\beta f L} \quad (\text{for } \tilde{L} = 0 \text{ and any } f), \tag{2.6}$$

through (2.3).

The second analytic expression is in the weakly stretched regime when f is small. Based on the energy-fluctuation theorem, one has a general relation,

$$\left\langle z^2 - \langle z \rangle^2 \right\rangle = \frac{\partial \langle z \rangle}{\partial \beta f} \tag{2.7}$$

For small forces the polymer behaves as a harmonic spring, hence, taking a linear relation between $\langle z \rangle$ and βf,

$$\langle z \rangle = \langle z^2 \rangle \beta f = \langle \mathbf{R}_{\mathrm{KP}}^2 \rangle \beta f / 3 \tag{2.8}$$

where

$$\langle \mathbf{R}_{\mathrm{KP}}^2 \rangle = 2\lambda L K(\lambda / L) \tag{2.9}$$

together with

$$K(x) = 1 - x + x \exp(-1/x) \tag{2.10}$$

gives the Kratky-Porod expression for the mean square end-to-end distance of an unstretched, free WLC [54]. The extension can be conveniently expressed by

$$\frac{\langle z \rangle}{L} = \frac{\tilde{f}}{3} \quad (\text{for } \tilde{f} \ll 1 \text{ and any } \tilde{L}) \tag{2.11}$$

in which a dimensionless

$$\tilde{f} \equiv \langle \mathbf{R}_{\mathrm{KP}}^2 \rangle \beta f / L \tag{2.12}$$

is defined. Using the Kraky-Porod mean squared end to end distance here scales out stretching dependence on the size of the polymer in question, allowing a direct comparison between them on the same plots, as seen later in figure 2.3. In conjunction with the reduced $\tilde{L}$ defined in (2.2), these two are used in Fig. 2.1 as the basic system parameters.

The third analytic solution is in the strongly stretched regime when $\tilde{f} \gg 1$. In this case, the external potential term in (2.1), $\cos\theta$, is approximated by $1 - \theta^2/2$. Due to the quadratic nature of the potential in θ, the partition function can be exactly evaluated by carrying out a path integral, based on the same approach as in the original quantum-mechanical problem for a simple harmonic potential formulated by Feynman [69]. The force-extension relation for strong stretching can then be deduced [5],

$$\frac{\langle z \rangle}{L} = 1 - \frac{1}{\beta f L} D\left(L \sqrt{\frac{\beta f}{\lambda}} \right) \quad (\text{for } \tilde{f} \gg 1 \text{ and any } \tilde{L}) \tag{2.13}$$

where

$$D(x) = \left[1 + x \coth(x) \right] / 2 \tag{2.14}$$

defines key strongly stretched behaviour. The exact region of validity of the above is illustrated in Fig. 2.1(b) and further discussed in section 2.3.2

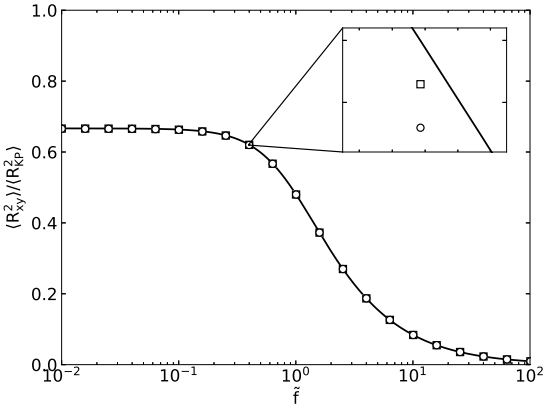

Figure 2.2: An example of Richardson extrapolation for the $\langle R^2_{xy}\rangle$, the mean squared end-to-end distance in the direction perpendicular to the applied force (see section 2.3.4), GSD long chain limit data. The solid black line is the final numerical data set, the circles are the solution from a 500×500 matrix (1/50 of points shown), while the squares are for a 1000×1000 matrix (1/50 of points shown). The error scaling on the black line is an order better than that for the squares and circles from the application of Richardson extrapolation. The inset shows a zoom in of one set of data points.

2.3.2 Numerical Results

The partial differential equation (2.5) admits no closed form solution in other regions, and must be solved numerically to obtain the extension-force curves over the full parameter range of $[\tilde{L}, \tilde{f}]$. To do this we employ the Crank-Nicolson method to solve the differential equation for the propagator, based on dividing the variable domains t and θ into a finite grid system to carry out the numerical computation using finite difference approximations of the differential operators [70]. The Crank-Nicolson method is the average of Forward and Backward Euler methods in t, and our scheme uses a central difference to handle the derivatives in θ. The methods and the types of differences are discussed in section 1.5. Once the numerical representation of the propagator $q(\theta, t)$ is obtained, it is numerically integrated using Simpson's method to find the partition function Q via equation (2.4). A numerical derivative of Q is then taken with respect to the force, in order to obtain the average extension through equation (2.3).

We generate 4 sets of data, dividing the grid into combinations of 1×10^6 or 0.5×10^6 points in t, and 1×10^3 or 0.5×10^3 points in θ, then apply Richardson extrapolation (see section 1.5.5) in both t and θ to reduce the errors due to the finite $\Delta\theta$, and Δt [58]. An example of the process for the long chain $\tilde{L} \gg 1$ limit (independent of t) is shown in figure 2.2, the error scaling of $\langle R^2_{xy}\rangle$ is improved from $\mathcal{O}(\Delta\theta)$ to $\mathcal{O}(\Delta\theta^2)$.

The numerical solution is presented in Fig. 2.3(a) as a function of $\tilde{f}$ for

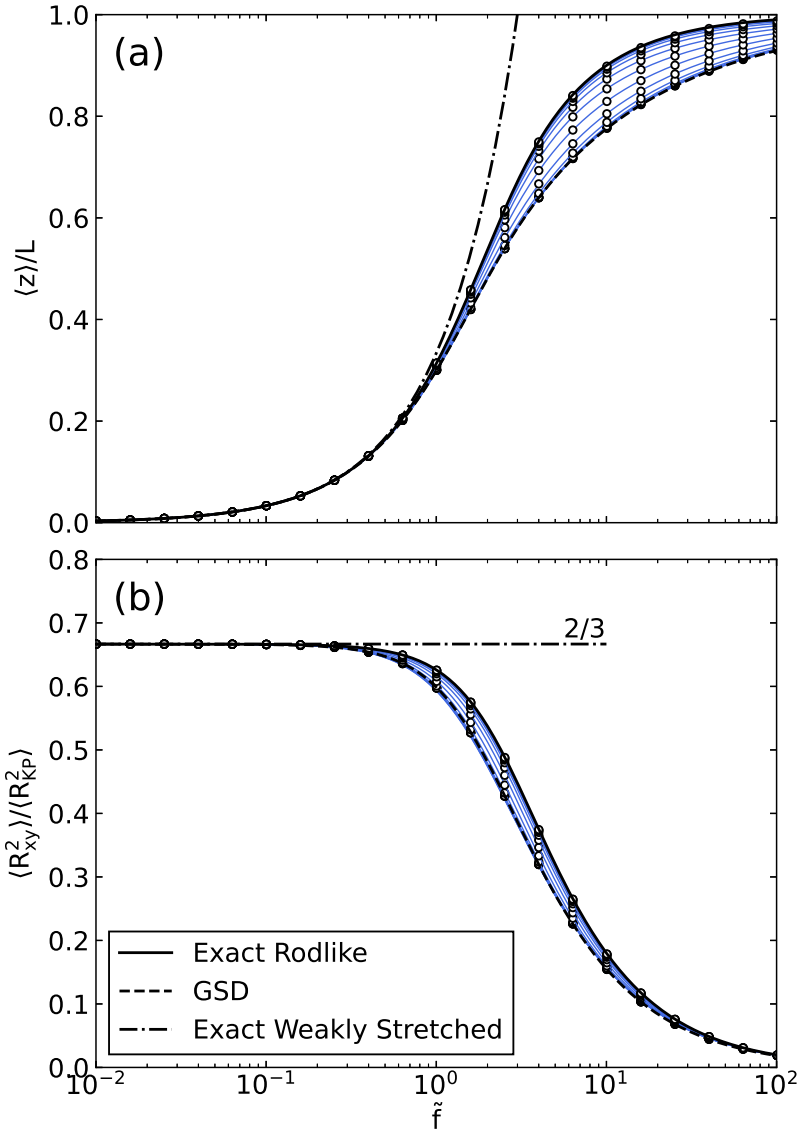

Figure 2.3: Full numerical solution (circles) and our interpolation formula (blue lines) for (a) the extension $\langle z\rangle/L$, and (b) the mean square end-to-end distance projected on the xy plane, $\langle R^2_{xy}\rangle/\langle R^2_{KP}\rangle$. The numerical solution is arranged for selected $\tilde{L} = 2^{-7}$ (top curve), $2^{-6}, \ldots, 2^5$ (bottom curve), The blue lines connecting the data points are our interpolation formulae (2.21) and (2.46). The solid lines represent the exact rodlike limits Eqs. (2.6) and (2.28), the dashed lines the GSD results (see appendix A), and the dash-dot lines the analytic weakly stretched limits Eqs. (2.11) and (2.30).

$\tilde{L} = 2^{-7}, 2^{-6}, \ldots, 2^{5}$ and is available online [71]. In all cases the estimated error bars are smaller than the linewidth of the curves or size of the symbols used in the figures. With the use of $\tilde{f}$ defined in (2.12), all data points in the full range $[\tilde{L}, \tilde{f}]$ can be accommodated within a single plot. For comparison, the exact solution, (2.6), for the rodlike limit, and (2.11), for the weakly stretched regime, are plotted as the solid and dot-dashed curves in the figure. The long chain results of Marko and Siggia are reproduced as the dashed line in figure 2.3 (a), while the dashed line in figure 2.3 (b) are presented in this work for the first time, using a very similar approach. The technique used is known as the ground state dominance (GSD) approach, and is discussed in appendix A.

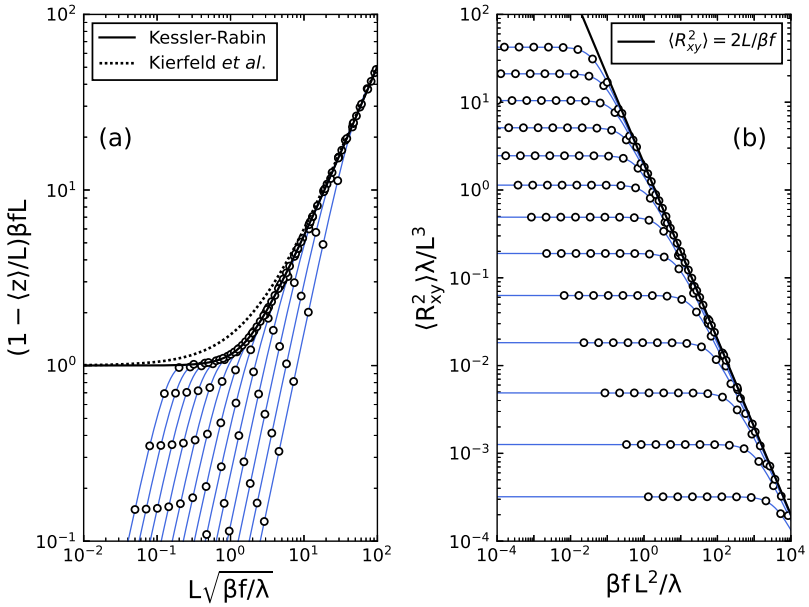

Figure 2.4: Comparison between the analytic expressions in the strong force regime and the numerical solutions (circles) for $\tilde{L} = 2^{-7}$ (rightmost curve in (a) and topmost curve in (b)), $2^{-6} \ldots 2^{5}$ (leftmost curve in (a) and bottom most curve in (b)). In (a) the solid curve represents the function $D(\zeta)$ in eq. (2.14) and the dotted line eq. (40) in Ref. [6]. The result from Ref. [6] shows agreenments in the limits of $\tilde{L} \gg 1$ and $\tilde{L} \ll 1$, but does not capture the results in the intermediate regime, as is visible in (a). In (b), the solid curve is given by (2.30), The connecting blue lines are our interpolation formulae, (2.21) and (2.46).

To compare against the exact stronlgy stretched expression (2.13), $(1 - \langle z \rangle / L)\beta f L$ is plotted as a function of $\zeta = L\sqrt{\beta f/\lambda}$ for various $\tilde{L}$. According to (2.13), a single solid curve is drawn in Fig. 2.4(a) for all values of $\tilde{L}$. The overlap between the numerical data and the solid curve indicates the re-

gion of applicability of (2.13). Taking 1% agreement with the numerical data as the criterion, the strongly stretching regime is quantitatively established in Fig. 2.1(b) by the line-shaded area on the right. While (2.13) is validated by our numerical results, another analytic expression for the force-extension relation, Eq. (40) in Ref. [6], is shown to contain flaw in the intermediate region, as illustrated by the dotted curve in Fig. 2.4 (a).

The validity of (2.11) for the weakly stretched regime can be assessed in a similar way. Again taking 1% agreement as the criterion, Eq. (2.11) (the dot-dashed curve in Fig. 2.3 (a)) and the numerical data overlap below $\tilde{f} \approx 0.3$ for all $\tilde{L}$, within the weakly stretched region displayed by the line-shaded region on the left in Fig. 2.1(b).

2.3.3 Interpolation Formulae

Although the full numerical solution is available, and the theory facilitates calculations for arbitrary values of L, λ and f if desired, it is convenient to have an accessible form of the results which does not require large computation or a deep understanding of the underlying theory. A summary of the results can be obtained through the use of an interpolation formula, which interpolates between the known exact solutions in order to obtain an approximation of the full results. Many interpolation formulae have been proposed since the first suggestion by Marko and Siggia for $\tilde{L} \gg 1$ [2]

$$\beta f \lambda = \frac{\langle z \rangle}{L} + \frac{1}{4(1 - \langle z \rangle / L)^2} - \frac{1}{4} \tag{2.15}$$

attempting to capture the area between the weakly stretched and strongly stretched regions in a closed form. Notably, within the same $\tilde{L} \gg 1$ limit, several improvements were made. Petrosyan proposed both force-extension

$$\beta f \lambda = \frac{\langle z \rangle}{L} - 0.8 \left(\frac{\langle z \rangle}{L} \right)^{2.15} + \frac{1}{4(1 - \langle z \rangle / L)^2} - \frac{1}{4} \tag{2.16}$$

and extension-force

$$\begin{aligned} \frac{\langle z \rangle}{L} = \frac{4}{3} - \frac{4}{3(\beta f \lambda + 1)^{1/2}} \\ + \frac{(\beta f \lambda)^{1.62}}{3.55 + 3.8(\beta f \lambda)^{2.2}} \\ - \frac{10 \exp[(900/\beta f \lambda)^{1/4}]}{(\beta f \lambda)^{1/2} (\exp[(900/\beta f \lambda)^{1/4}] - 1)^2} \end{aligned} \tag{2.17}$$

formulae, both with less than 1% relative error [4]. Bouchiat et al. proposed a more accurate force-extension formula using a seventh-order polynomial, giving at most 0.01% relative error [3].

$$\beta f \lambda = \frac{\langle z \rangle}{L} + \frac{1}{4(1 - \langle z \rangle / L)^2} - \frac{1}{4} + \sum_{i=2}^{i \leq 7} \alpha_i \left(\frac{\langle z \rangle}{L} \right)^i, \tag{2.18}$$

where $\alpha_2 = -0.5164228$, $\alpha_3 = -2.737418$, $\alpha_4 = 16.07497$, $\alpha_5 = -38.87607$, $\alpha_6 = 39.49944$, $\alpha_7 = -14.17718$.

For the small-$\tilde{L}$ regime, Kessler and Rabin proposed an extension-force interpolation formula [5]. Their expression,

$$\frac{\langle z\rangle}{L} = -\frac{1}{2\beta f L} - \frac{1}{2\sqrt{\beta f \lambda}}\coth\left(L\sqrt{\frac{\beta f}{\lambda}}\right) + \coth(\beta f L) - \frac{1}{6}\frac{L}{\lambda}\left[\coth(\beta f L) - \frac{\beta f L}{\sinh^2(\beta f L)} - 1\right], \quad (2.19)$$

can be compared with our numerical result, shown in Fig. 2.1(f), and is valid over the entire strongly stretched regime, due to their success of finding the analytic result. The same formula, however, gives the wrong $\langle z\rangle/L$ in the weakly stretched, large $\tilde{L}$ region (red in Fig. 2.1(f)), where (2.19) yields an unphysical value, due to their focus on capturing the rodlike and strongly stretched limits, at the expense of the flexible limit.

For the entire $[\tilde{L}, \tilde{f}]$ space, Kierfeld et al. suggested using the force-extension interpolation formula [6],

$$\beta f = \frac{1}{4\lambda}\left[\frac{1}{(1-\langle z\rangle/L)^2} - 1\right] + \frac{1}{L}\left[\frac{1}{1-\langle z\rangle/L} - 1\right] + \frac{\langle z\rangle}{L}\left[\frac{3}{2\lambda K(\lambda/L)} - \frac{1}{L} - \frac{1}{2\lambda}\right]. \quad (2.20)$$

This is evaluated here against our numerical solution as well. The original formula took the large and small $\tilde{f}$ behaviour into consideration, hence it agrees well with the numerical solution in these two regions. On the other hand, it produces a large error in the intermediate $\tilde{f}$ regime, which can be partially traced back to the problematic handling of intermediate force regime demonstrated in Fig. 2.4(a).

Overall, the quality of the above interpolation formulae is evaluated and summarized in Fig. 2.1(c)-(g). As the numerical solution presented in this chapter is a function of the force, the force extension formulae were numerically inverted (2.15, 2.18, 2.20) in order to present a meaningful perspective. All equations in the above have been updated with the exact notation used in the current work.

While the numerical solution from the full-WLC is available and tabulated for specific $\tilde{L}$ and $\tilde{f}$ values [71], it can be represented within 1% globally by a new interpolation formula. Using the expression for the rodlike limit as a template

$$\langle z\rangle/L = \coth(f^\dagger) - 1/f^\dagger \quad \text{(for any } [\tilde{L}, \tilde{f}]\text{)} \quad (2.21)$$

Table 2.1: Numerical values of the coefficients in Eqs. (2.21) and (2.46).

	a_0	a_1	a_1'
Eq. (2.21)	1.1268	0.3277	0.2127
Eq. (2.46)	8.2600	1.4868	-0.2576
	b_0	b_1	b_1'
Eq. (2.21)	0.3843	-0.2574	0.7261
Eq. (2.46)	7.6606	2.5013	0.0002
	c_0	c_1	c_1'
Eq. (2.21)	0.9586	-0.2030	1.3795
Eq. (2.46)	0.0796	0.2170	-0.7154

is proposed, where a rescaled force

$$f^\dagger = \tilde{f}\frac{1 + A_1(\tilde{L})\tilde{f} + A_2(\tilde{L})\tilde{f}^2 + A_3(\tilde{L})\tilde{f}^3}{1 + a_0\tilde{f} + b_0\tilde{f}^2 + A_3(\tilde{L})D(\zeta)\tilde{f}^3}. \tag{2.22}$$

is defined. The A-functions are expressed by

$$A_1 = \frac{a_0 + a_1K(\lambda/L)}{1 + a_1'K(\lambda/L)}, \quad A_2 = \frac{b_0 + b_1K(\lambda/L)}{1 + b_1'K(\lambda/L)},$$
$$A_3 = \frac{c_0 + c_1K(\lambda/L)}{1 + c_1'K(\lambda/L)}, \tag{2.23}$$

with the functions D and K given by (2.14) and (2.10) respectively, and $\zeta = L(\beta f/\lambda)^{1/2}$. All three known analytic expressions, for the rodlike, weakly stretched, and strongly stretched regimes, are exactly recovered from this proposal. The coefficients are determined by fitting to the full data set and are listed in Table 2.1. The formula accurately captures the numerical $\tilde{L} \gg 1$ and finite $\tilde{L}$ results, with the accuracy being within 1% of the numerical data, globally.

2.3.4 Perpendicular Projection of the Mean Squared End-to-end Distance

The rest of this chapter presents the theoretical calculations, for the mean squared end-to-end distance, projected on the xy-plane, $\langle \mathbf{R}_{xy}^2 \rangle$. Except for the trivial rodlike and weakly stretched limits, little has been presented on this in the literature.

Analytic Solutions

The rodlike limit, $\tilde{L} \ll 1$, is relatively straightforward. As previously discussed for the extention, the propagator under the rodlike limit $\tilde{L} \to 0$ is

$$q(\theta, t) = e^{Lt\beta f \cos\theta} \tag{2.24}$$

Calculation of the associated partition funciton through equation (2.4) gives

$$\frac{Q}{V} = \int_0^\pi e^{\beta L f \cos\theta} \sin\theta \, \mathrm{d}\theta = \frac{2 \sinh \beta f L}{\beta f L} \tag{2.25}$$

One can then use the parition function to calculate the average of $\mathbf{R}_{xy}^2$

$$\langle \mathbf{R}_{xy}^2 \rangle = \frac{1}{Q} \int \mathbf{R}_{xy}^2 e^{-\beta H} \, \mathrm{d}\mathbf{u} \, \mathrm{d}\mathbf{r} \tag{2.26}$$

$$= \frac{V}{Q} \int_0^\pi (L \sin\theta)^2 e^{\beta L f \cos\theta} \sin\theta \, \mathrm{d}\theta \tag{2.27}$$

Subsituting the parition function and evaluating the integral then yields

$$\frac{\langle \mathbf{R}_{xy}^2 \rangle}{L^2} = \frac{2}{\beta f L} \left(\coth \beta f L - \frac{1}{\beta f L} \right) \quad (\tilde{L} \ll 1, \text{ any } f). \tag{2.28}$$

which is the rodlike result for the projection of the squared end-to-end distance in the direction perpendicular to the stretching.

In the weakly stretched regime, the conformational properties reduce to those described by the Kratky-Porod expression (eq. (2.9)), hence

$$\frac{\langle \mathbf{R}_{xy}^2 \rangle}{\langle \mathbf{R}_{\mathrm{KP}}^2 \rangle} = \frac{2}{3}, \quad (\text{for } \tilde{f} \ll 1 \text{ and any } \tilde{L}). \tag{2.29}$$

These limits are well known.

A derivation based on the two-point correlation function to obtain the expression for the strongly stretched regime can be done, as presented in appendix B. The same Feynman integral of the quadratic potential well, used in Ref. [5] for the calculation of the partition function, can be used here, but in a more involved algebraic exercise. The final result is a surprisingly simple relation, $\langle \mathbf{R}_{xy}^2 \rangle = 2L/\beta f$ for all $\tilde{L}$, which can be recast in the form

$$\frac{\langle \mathbf{R}_{xy}^2 \rangle}{\langle \mathbf{R}_{\mathrm{KP}}^2 \rangle} = \frac{2}{\tilde{f}} \quad (\text{for } \tilde{f} \gg 1 \text{ and any } \tilde{L}), \tag{2.30}$$

structurally simpler than (2.13).

Numerical Solutions

As in the case for the extension, beyond these three regimes a numerical approach must be taken, as there is no analytic solution. To numerically calculate $\langle \mathbf{R}_{xy}^2 \rangle$, we perturb the original problem by adding an auxiliary field

$$H' = -\int_0^1 L u_x(t) \, \mathrm{d}t \tag{2.31}$$

to the Hamiltonian (Eq. 2.1) with magnitude ϵ, giving $H = H_0 + \epsilon H'/\beta$ where the subscript 0 referes to the original problem without the newly added external field. The new Hamiltonian is then

$$\beta H = \int_0^1 \left[\frac{\lambda}{2L} \left| \frac{\mathrm{d}\mathbf{u}(t)}{\mathrm{d}t} \right|^2 - \beta L f u_z(t) - \epsilon L u_x(t) \right] \mathrm{d}t. \tag{2.32}$$

Using the energy fluctuation theorem in classical mechanics, we have

$$\left\langle [H']^2 - \langle H' \rangle^2 \right\rangle = -\frac{\partial}{\partial \epsilon} \langle H \rangle \tag{2.33}$$

Because of the symmetry of the distribution for $\epsilon = 0$, we have

$$\left\langle [H']^2 \right\rangle \Big|_{\epsilon=0} = -\frac{\partial}{\partial \epsilon} \langle H \rangle \Big|_{\epsilon=0} \tag{2.34}$$

From the definition of H', we can then see that

$$\left\langle [H']^2 \right\rangle = L^2 \langle u_x^2 \rangle = \frac{1}{2} \langle \mathbf{R}_{xy}^2 \rangle \tag{2.35}$$

or, with the help of equation (2.34),

$$\langle \mathbf{R}_{xy}^2 \rangle = 2L^2 \langle u_x^2 \rangle = 2L^2 \frac{\partial}{\partial \epsilon} \langle u_x \rangle \Big|_{\epsilon=0} \tag{2.36}$$

where all the averaging is performed with the full probability distribution of the original Hamiltonian plus the auxillary field. As $u_x = \sin\theta \cos\phi$, the new propagator under the perturbing field now satisfies

$$\frac{\partial}{\partial t} q(\theta, t) = \left[\tilde{L} \left(\frac{1}{\sin\theta} \frac{\partial}{\partial \theta} \sin\theta \frac{\partial}{\partial \theta} \right) + \beta L f \cos\theta + \epsilon L \sin\theta \cos\phi \right] q(\theta, t) \tag{2.37}$$

In order to compute $\langle u_x \rangle$, the propagator from the above equation can be used to calculate the monomer density distribution ρ (see section 1.4). We first expand both the propagator q and density distribution ρ to first order in ϵ, giving $q = q_0 + \epsilon q_1 \cos\phi$ and $\rho = \rho_0 + \epsilon \rho_1 \cos\phi$. The ϕ dependence has been explicitly included for clarity. The expanded forms are then substituted into the definition of the density distribution

$$\rho = \frac{1}{B} \int_0^1 q(\theta, t) q^*(\theta, t) \, \mathrm{d}t \tag{2.38}$$

which after matching powers of ϵ gives

$$\rho_0 = \frac{1}{B} \int_0^1 q_0(\theta, t) q_0^*(\theta, t) \, \mathrm{d}t \tag{2.39}$$

$$\rho_1 = \frac{1}{B} \int_0^1 \left[q_0(\theta, t) q_1^*(\theta, t) + q_0^*(\theta, t) q_1(\theta, t) \right] \mathrm{d}t \tag{2.40}$$

where $q_0^*(\theta,t) = q_0(\theta,1-t)$ $q_1^*(\theta,t) = q_1(\theta,1-t)$ are the complementary propagators. The normalization factor B can be obtained through equation (2.39). The propagator $q_1(\theta,t)$ associated with the external field can be obtained by substituting the expanded form into equation (2.37), which yields

$$\frac{\partial}{\partial t}q_1(\theta,t) = \left[\frac{L}{2\lambda}\frac{\partial^2}{\partial\theta^2} + \beta f L\cos\theta\right] q_1(\theta,t) + \sin\theta\cos\phi\, q_0 \tag{2.41}$$

Once both propagators have been obtained, the average $\langle\sin\theta\cos\phi\rangle$ can then be obtained through

$$\langle\sin\theta\cos\phi\rangle = \int_0^{\pi}\int_0^{2\pi}\rho(\sin\theta\cos\phi)\sin\theta\,\mathrm{d}\theta\mathrm{d}\phi \tag{2.42}$$

which, because the ρ_0 distribution is symmetric in ϕ, reduces to

$$\langle\sin\theta\cos\phi\rangle = \epsilon\pi\int_0^{\pi}\rho_1\sin^2\theta\,\mathrm{d}\theta \tag{2.43}$$

Therefore, going back to equation (2.36), the projection of the mean squared end-to-end distance in the direction perpendicular to the stretching is given by

$$\langle\mathbf{R}_{xy}^2\rangle = 2L^2\frac{\partial}{\partial\epsilon}\langle\sin\theta\cos\phi\rangle \tag{2.44}$$

$$\frac{\langle\mathbf{R}_{xy}^2\rangle}{L^2} = 2\pi\int_0^{\pi}\rho_1\sin^2\theta\,\mathrm{d}\theta \tag{2.45}$$

This procedure is similar to that described in detail in Ref. [72]. The partial differential equations are tackled by the Crank-Nicolson method and Richardson extrapolation, as described previously, although the t spacing is increased by a factor of 10 to avoid computational issues.

As before, using $\tilde{f}$ as the reduced force, the entire data can again be captured in a single plot, shown in Fig. 2.3(b) by the circular symbols. Plotted alongside are the exact solutions for the rodlike limit, (2.28) and the weakly stretched region (2.29).

Based on the theory and data we propose a global interpolation formula for $\langle R_{xy}^2\rangle$ covering the entire $[\tilde{L},\tilde{f}]$ plane, to our knowledge the first of its kind in the literature. Using (2.28) as a template, we propose

$$\frac{\langle\mathbf{R}_{xy}^2\rangle}{\langle\mathbf{R}_{\mathrm{KP}}^2\rangle} = \frac{2}{f^\dagger}\left(\coth f^\dagger - \frac{1}{f^\dagger}\right). \tag{2.46}$$

The definition of the reduced force, $f^\dagger$, is the same as in (2.22) but $D \equiv 1$ is enforced. It can be shown, by taking the asymptotic limits, that this representation fully recovers the analytic expressions, (2.28), (2.29) and (2.30). The fitted coefficients are listed in Table 2.1. This global interpolation formula represents our numerical $\langle\mathbf{R}_{xy}^2\rangle$ data with a maximum error of 6×10^{-4}.

2.4 Summary

In summary, taking the the Green's function approach to solving the WLC model, a full high-precision numerical solution of the forced stretching problem of a wormlike chain, covering a large range of $L/2\lambda$ and f, is presented. The solution clearly illustrates the crossover from weakly stretched to strongly stretched, and from rodlike to long chain behaviour. This allowed assessment of the validity of known analytic solutions in asymptotic regimes as well as the efficacy of several interpolation formulae between them. A global extension-force interpolation formula that reproduces all known exact limits while matching the numerical data to high accuracy, was also presented.

Calculations in this chapter were done by fixing the force, then computing the ensemble average of the extension from the Gibbs free energy. Another theoretical approach is to fix the extension and calculate the ensemble average of the force required to maintain that extension through the Helmholtz free energy. For a stretched WLC, these two correspond to two different types of experiments, where the difference between the force-extension curves diminishes only in the thermodynamic limit of $\tilde{L} \to \infty$ and strongly stretched regime of $\tilde{f} \gg 1$ [73].

The starting point of the theoretical approach taken here is exactly the same as those used in Refs. [2–6]. The interpolation formulae compared in section 2.3.3 differ from each other due to approximations made in the mathematical representations. A key quantity used in calculating the total partition function is the propagator that takes into account all polymer configurations with a fixed terminal direction. A recent publication [74] focuses on the conditional partition function of a two-dimensional, loop-constrained WLC, which is a different type of Green's function.

The theoretical results presented here are for a stretched polymer with free ends and no excluded-volume interactions. Hori et al. examined in detail the strongly stretched regime for the case where the polymer terminals are restricted to point in the same direction as the applied force, as well as for the case where the polymer's end-to-end vector is forced to be collinear with the applied force [65]. An experimental discussion on the collinear case can be found in [45]. The effects of excluded volume for the discrete wormlike chain model with free ends over the full parameter regime were examined by computer simulations in [67], which showed a decrease of its importance as finite length effects dominate, which was the main consideration in this chapter.

Chapter 3

Wrapping of Carbon Nanotubes by Wormlike Chains

The helical wrapping of single walled carbon nanotubes (SWNTs) by long polymer segments is an experimentally well studied problem owing to the ability of the polymers to effectively solvate and separate individual nanotubes in solution, without affecting their underlying electronic properties. However, there is only one theoretical model for this system, by Lundberg and Strano [25]. This chapter analyses these systems by presenting the first theory based on the Green's function approach, using the standard wormlike (WLC) chain polymer model, and shows that it accurately predicts the experimental helix pitch for polymer wrapped nanotubes. The system is modelled as a polymer with persistence length λ confined to the surface of an infinitely long cylinder of radius R. Using the Green's function theory, a full numerical solution is obtained. Examining the limit of small R nanotubes, we find the exact pitch to be $P/R = (2\pi/0.975)(\lambda/R)^{1/3}$, which has the expected Odijk exponent for a tightly confined WLC system. An interpolation formula covering the experimental range is provided. The chapter is concluded by comparing to an existing theory, and discussing the differences. The contents of the chapter have been prepared for publication, but at the time of writing are yet unpublished.

3.1 Introduction

The helical wrapping of nanotubes has been recognized as an important problem for nanotechnology. The wrapping of single walled carbon nanotubes (SWNTs) in particular has received much experimental and theoretical study, owing to the beneficial effects on solvation and separation, with minimal modification to the underlying electronic properties. SWNTs are poorly soluble in both

water and organic solvents, and previous methods relied on techniques such as chemical modification of the tubes to facilitate solvation; by wrapping the nanotube with a polymer which is soluble in the solvent of interest (eg. water), the nanotube itself is readily solvated [46–51]. Polymer wrapping has proved particularly useful for the purification of SWNTs from commercial samples, as it allows the separation of semiconducting nanotubes with specific diameters [75, 76]. Polymer wrapping has also shown potential to improve certain applications of SWNTs, for example, developing sensitive CO_2 detectors [77], as well as potentially serving as material for solar cells [78].

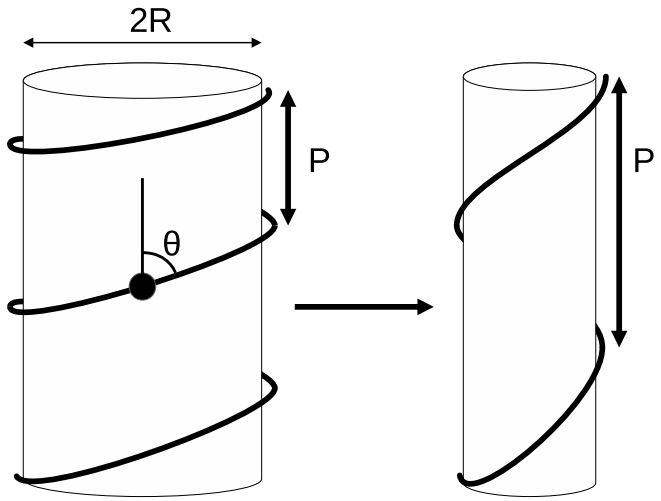

Figure 3.1: Schematic of a polymer wrapped nanotube. A smaller nanotube has a higher degree of confinement, resulting in a larger pitch (relative to the radius). For the long polymers considered here, the exact behaviour depends on the polymer stiffness and nanotube radius in tandem.

To form a comprehensive understanding of a polymer wrapped SWNT, two problems need to be examined. The first is the adsorption process, showing how the polymer becomes confined to the nanotube itself. The adsorption process where the polymer segment wraps around the nanotube, especially for single stranded DNA (ssDNA), has been studied extensively both experimentally and theoretically [79–84].

This chapter focuses on the second problem: what is the adopted conformation of the polymer after it has adsorbed to the nanotube surface? Although the adsorbed polymers can adopt a hairpin like structure, the lowest energy conformation is known to be a helix, and a polymer allowed to slowly adsorb onto the surface spontaneously adopts a helical conformation [81, 84]. Helically wrapped SWNTs have been observed experimentally and by molecular dynamics simulations (MD) for several polymers, with ssDNA ($\lambda \approx 1.5$) as a prominent

choice [7–15]. While some experimental results were also verified using MD simulations, these approaches are limited to specific system parameters.

In this work, the wormlike chain (WLC) polymer model is used to describe a semi-flexible polymer helically wrapping the surface of a nanotube, and to compute its pitch as a function of the nanotube radius and polymer stiffness. The polymer is considered to be fully adsorbed to the nanotube surface, and therefore the problem becomes effectively 2D. The surface attraction between the nanotube's carbon lattice and the polymer's constituent monomers constrains the chain to the plane of the nanotube's surface, but allows it to move freely within this plane. The optimal configuration is then determined through a competition of entropic factors, which drive the system towards a random coil, and energetic factors, where the forced bending around the tube surface raises the free energy of the system. The WLC is a fundamental model, and has been applied to good effect on confinement problems before [72, 85]. Section 3.3.1 describes the basic theory, and shows that when applied to a long polymer with contour length L much larger than it's persistence length λ ($L \gg \lambda$) the model accurately reproduces experimental observations. For small nanotubes, the pitch follows the expected Odijk power law, the exact form of which we derive here.

The only other theory that models the same type of system was published recently by Lundberg and Strano [25]. This is discussed in section 3.3.4, and the results of both theories are compared and differences examined.

3.2 Wormlike Chain on a Curved Surface

Again, the WLC model is used to model the system. In a typical experimental system, the nanotube length is much larger than the contour length L of the polymer, and edge effects near the ends of the SWNT can be ignored. Hence, we represent the nanotube as an infinitely long cylinder of radius R, the symmetries of which remove the dependence on the position $\mathbf{r}(t)$ from the problem, and reduce the orientation tangent vector $\mathbf{u}(t)$ to depend only on the angle θ from the polymer tangent to the z axis of the nanotube $\mathbf{u} = \mathbf{u}(\theta)$. As will be shown, for a long polymer, the ratio of the persistence length to the nanotube radius λ/R is the only system parameter that controls the conformational behaviour. We will consider here the long chain approximation that $L \gg \lambda$, which we find to be adequate to capture the experimental results.

When the polymer is confined to the nanotube, the external field in the WLC Hamiltonian given in equation (1.13), $U[\mathbf{r}(t), \mathbf{u}(t)]$ becomes the confining potential, representing a harmonic bending energy penalty proportional to the squared curvature of the nanotube surface

$$U[\mathbf{r}(t), \mathbf{u}(t)] = \frac{L}{2\lambda} \left(\frac{\lambda}{R} \right)^2 \sin^4(\theta) \tag{3.1}$$

representing the energy cost associated with confining the polymer to the surface of the nanotube. To determine the helix pitch for a given system, the monomer

density distribution for the polymer

$$\rho(\theta) = B^{-1} \int_0^1 q(\theta, t) q(\theta, 1-t) \mathrm{d}t \tag{3.2}$$

as discussed in section 1.4, is used. In equation 3.2, $q^*(\mathbf{r}, \mathbf{u}, t) = q(\theta, 1-t)$ due to the symmetry of the problem. The prefactor B is a normalization factor ensuring that

$$\int_{-\pi}^{\pi} \rho(\theta) \mathrm{d}\theta = 1 \tag{3.3}$$

The modified diffusion equation for the propagator under the curvature in equation 3.1 is [53, 86]

$$\frac{\partial}{\partial t} q(\theta, t) = \left[\frac{L}{2\lambda} \frac{\partial^2}{\partial \theta^2} - \frac{L}{2\lambda} \left(\frac{\lambda}{R} \right)^2 \sin^4 \theta \right] q(\theta, t) \tag{3.4}$$

To find $q(\theta)$ from (3.4), we consider an expansion of $q(\theta)$ in the eigenbasis of the right-hand side of (3.4)

$$\frac{\partial \psi_i}{\partial t} = -\mu L \psi_i \tag{3.5}$$

Taking the long chain limit $L \to \infty$ (with λ fixed), allows application of the ground state dominance (GSD) theory (see appendix A), giving $q(\theta, t) = \psi_{min}(\theta, t)$. The eigenvectors ψ are numerically computed by discretizing the operator

$$A = \left[\frac{\partial^2}{\partial \theta^2} - \left(\frac{\lambda}{R} \right)^2 \sin^4 \theta \right] \tag{3.6}$$

Numerical Method

The discretization of the A operator is done using a central difference scheme to numerically approximate $\partial^2/\partial\theta^2$, as discussed in section 1.5.1. The domain, θ, is discretized into a grid with 10^6 points. The discretized operator A is represented on this grid as a square sparse matrix with 3×10^6 elements, and the eigenvector corresponding to the smallest eigenvalue μ is numerically determined. This gives the GSD propagator $q(\theta, t) = \psi_{min}(\theta, t)$. Full details on the GSD theory used are given in appendix A.

3.3 Results

3.3.1 Helix Pitch and Comparison to Experiment

The pitch P of a long polymer with persistence length λ in a helical configuration on the surface of a SWNT of radius R can be found through

$$\frac{P}{R} = \frac{2\pi}{\tan(\theta)} \tag{3.7}$$

Where the angle θ that the tangent vector of the polymer $\mathbf{u}$ makes with the vertical defines the helix. The average helix angle is computed using the density distribution $\rho(\theta)$ (see sections 1.4 and 3.2) that is numerically computed under the GSD scheme (see appendix A)

$$\langle|\theta|\rangle = \int_{-\pi}^{\pi} |\theta|\rho(\theta)\mathrm{d}\theta \tag{3.8}$$

The absolute value is taken to avoid the $\langle\theta\rangle = 0$ symmetry of the system. The normalization factor B for the density distribution ρ under GSD is

$$B = \frac{1}{2}\int_{-\pi}^{\pi} q(\theta,t)q(\theta,1-t)\mathrm{d}\theta\mathrm{d}t = \frac{1}{2}\int_{-\pi}^{\pi} \psi_{min}(\theta)^2\mathrm{d}\theta \tag{3.9}$$

where the factor of $1/2$ is included to compensate for over counting helices related through angular rotations of $\theta' = \pi - \theta$, which are indistinguishable by experimental pitch measurements (the pitch of a left-handed helix is the same as that of a right-handed helix), but are distinguishable through their θ in our base theory. Dividing the configuration space by the number of indistinguishable permutations in this way is analogous to the over counting of indistinguishable states in classical mechanics [39], and is required to compare our theory to experiment.

Once the average angle $\langle|\theta|\rangle$ of the helical conformation is determined using equation 3.8, the pitch of the average helix for a given value of λ/R is obtained through

$$\frac{P}{R} = \frac{2\pi}{\tan(\langle|\theta|\rangle)} \tag{3.10}$$

We computed the pitch for $\lambda/R \in [10^{-1}, 10^2]$, by taking a central difference discretization of (3.6) with 10^6 equally spaced points in $\theta \in [0, \pi/2]$ (exploiting the symmetry over the domain), and numerically computed its smallest eigenvalue and corresponding eigenvector, then used (3.2) and (3.8) under the GSD limit to obtain $\langle|\theta|\rangle$ and hence the associated pitch.

The results are given in Figure 3.2 as the solid black curve, compared against 10 different experimental and molecular dynamics studies for ssDNA, Chitosan, Alginic Acid, PNES, and PPES (the last two are abbreviations of chemical names, see the List of Abbreviation for the full definitions) [7–15]. The exact data points are presented in appendix C.2, along with their persistence lengths. Excellent agreement is seen with the data, save for two exceptions in the top left. These points correspond to atomic force microscopy (AFM) measurements by Zheng et al., and Campbell et al. [11, 12]. Both use the same ssDNA sequence, $(GT)_{30}$, and use nanotubes of similar radii. Zheng et al. posited that the repeating structure allowed two ssDNA segments to interact and form a "charge strip"; a single long polymer with both segments linked through hydrogen bonding [11]. If we assume this double ssDNA structure has a similar persistence length to dsDNA (~50 nm, or ~25× that of ssDNA) [87], then we see find the data (grey circles in figure 2.3) agrees with our WLC theory. Our

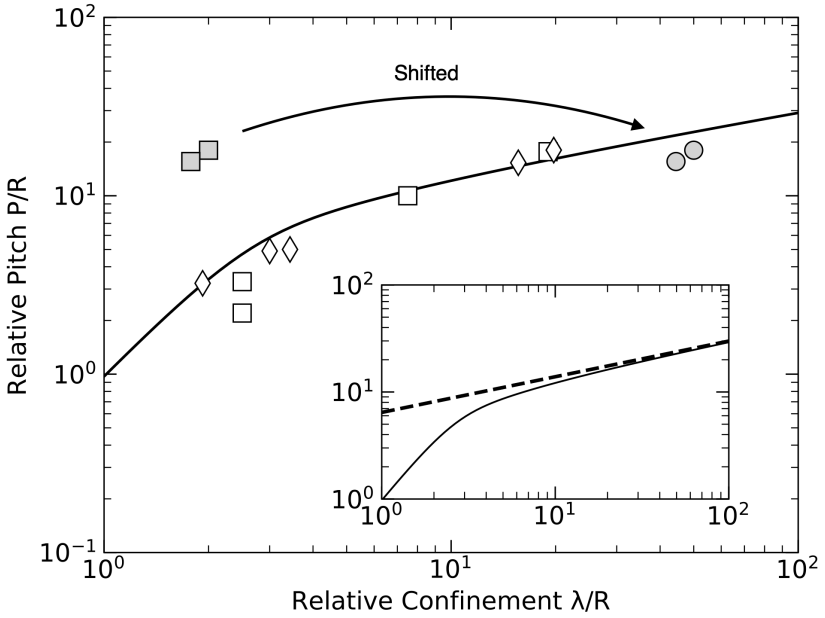

Figure 3.2: Comparison with data from 10 different studies in the literature, spanning 6 different polymer types. The square markers are experimental measurements [7–12], while the diamonds are simulations [9, 13–16]. The solid black curve is the numerical calculation done in this chapter. The grey circles (top right) are the data from Zheng et al. and Campbell et al. (top left squares), shifted to approximate the persistence length of the "charge strip" 2x ssDNA structure suggested by Zheng et al. [11, 12]. Details are discussed in the text. The persistence lengths for each of the polymers was estimated based on the experimental conditions and existing literature [17–24]. The inset shows the large λ/R scaling behaviour eq. (3.16) as the dashed line, and the numerical data as the solid black line.

results therefore support the existence of such a hydrogen bonded ssDNA dimer, as a double-stranded ssDNA structure should have a persistence length on the order of dsDNA ($\lambda \sim 50$nm). However, the existence of this "charge strip" structure has been disputed by other studies [80].

3.3.2 Small R Scaling

By examining eq. (3.6) for large λ/R, the scaling behaviour for small nanotubes can be deduced. For such cases, the strong confinement causes the density distribution to peak around $\theta = 0$, and so $\sin(\theta)$ can be well approximated by a first order Taylor expansion, giving

$$A \approx \left[\frac{\partial^2}{\partial \theta^2} - \left(\frac{\lambda}{R} \right)^2 \theta^4 \right] \tag{3.11}$$

Making the substitution $\theta = \zeta/\sqrt{\alpha}$ and balancing the terms gives $\alpha = (R/\lambda)^{-2/3}$ hence

$$\theta = \zeta \left(\frac{\lambda}{R} \right)^{-1/3} \tag{3.12}$$

Therefore, under the strong confinement $\lambda/R \gg 1$, the pitch defined in eq. (3.7) becomes

$$\frac{P}{R} = \frac{2\pi}{\langle|\theta|\rangle} = \frac{2\pi}{\langle|\zeta|\rangle} \left(\frac{\lambda}{R} \right)^{1/3} \tag{3.13}$$

where the average of the scaled angle $\langle|\zeta|\rangle$ is obtained by solving for the eigenfunction of

$$A_\zeta \approx \left[\frac{\partial^2}{\partial \zeta^2} - \zeta^4 \right] \tag{3.14}$$

and computing the average via the scaled density distribution $\rho_\zeta(\zeta)$, which is obtained using the same procedure used for the general density distribution ρ, as discussed in sections 3.2 and 3.3.1:

$$\langle|\zeta|\rangle = \int_{-\infty}^{\infty} |\zeta| \rho_\zeta(\zeta) \, \mathrm{d}\zeta \tag{3.15}$$

Numerically, we find $\langle|\zeta|\rangle = 0.975$, and so for polymers tightly confined to small nanotubes the wrapping pitch is

$$\frac{P}{R} = \frac{2\pi}{0.975} \left(\frac{\lambda}{R} \right)^{1/3} \tag{3.16}$$

This scaling is clearly seen for large λ/R, plotted as the dashed line in the inset in Figure 3.2. The scaling exponent 1/3 is the same as that derived by Odijk for a WLC trapped within a cylindrical pore [88]. This in turn then naturally defines the deflection length, the characteristic length between changes in the polymer configuration, as $\lambda_{\mathrm{def}} = P$.

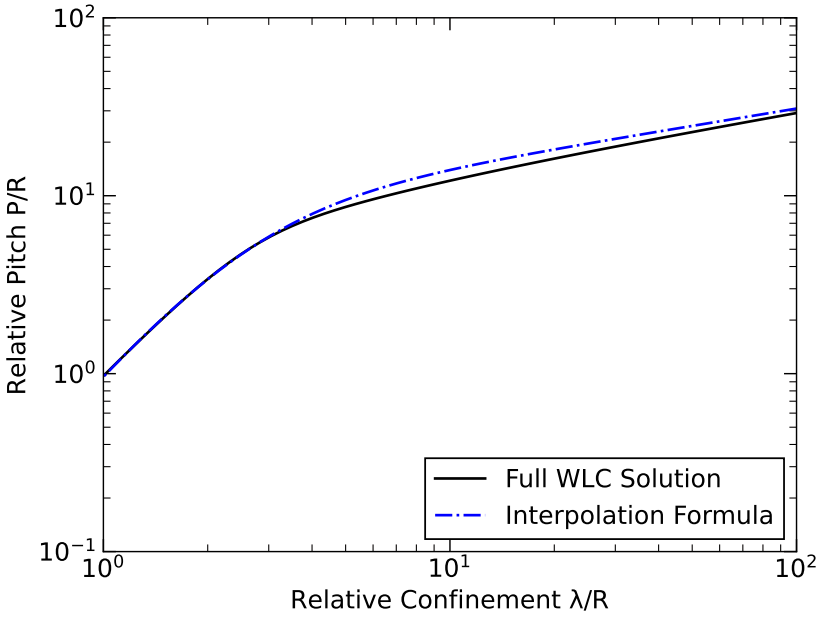

Figure 3.3: Comparison between the interpolation formula eq. (3.17), and the full numerical GSD solution. It closely matches the exact solution for strong and medium confinement, and gives a mean squared error of 1.5 over the numerical data range.

3.3.3 Interpolation Formula

The results of the WLC theory can be made more accessible through an interpolation formula, which approximates the results over the range of the parameter space valid to experiments. We find that the following form

$$\frac{P}{R} = Af(\lambda/R)\left(\frac{1+g(\lambda/R)}{1+Af(\lambda/R)}\right) \tag{3.17}$$

is able to adequately capture the results, with

$$f(x) = x^2 \tag{3.18}$$

$$g(x) = \frac{2\pi}{0.975}x^{1/3} \tag{3.19}$$

Because the exact small R result is known, we fit the linear large R region of the data, and obtain $A = 0.148$ as the numerical coefficient. A comparison between the two is given in Figure 3.3, showing excellent agreement with the WLC theory over the experimental region (from $\lambda/R \sim 2$ to $\lambda/R \sim 10^2$). Over the entire data range, the interpolation formula has a mean squared error of 1.5 in P/R.

3.3.4 Comparison Against Lundberg Theory

In addition to molecular dynamics simulations for specific systems, there has been another attempt to explain the observed helix pitch over a large range of system parameters. Lundberg and Strano constructed an implicit equation for the pitch based in part on approximations of the WLC model [25]. They also compare their theory to many of the same experimental measurements and molecular dynamics data that we do, and so a comparison between our two models is necessary. Although they made a good attempt, their use of an approximate WLC force, and a restriction of its direction to along the nanotube background were not fully justified, and so an examination of the problem from the perspective of the well established WLC model is valuable. We also note that we were unable to replicate the literature data points listed by Lundberg and Strano using the references given, and so our own interpretation of the studies cited in the work was required.

Pitch measurements were taken directly from the papers of interest. When a persistence length was provided in these works for the studied system, it was used. When a value for the persistence length was not given, it was estimated using a separate study on the polymer system of interest, and the change in persistence length due to salt concentration was taken into account using experimental measurements. Hence, it is believed that the data points presented in Figure 3.2 are accurate. All data points used can be found in the appendix C.2, and details on the numerical results of Lundberg and Strano reproduced from their theory is given in appendix C.1.

Both theories are compared, the numerical solution to equation (3.7) in this chapter, and the numerical solution to their equation (23). These are plotted

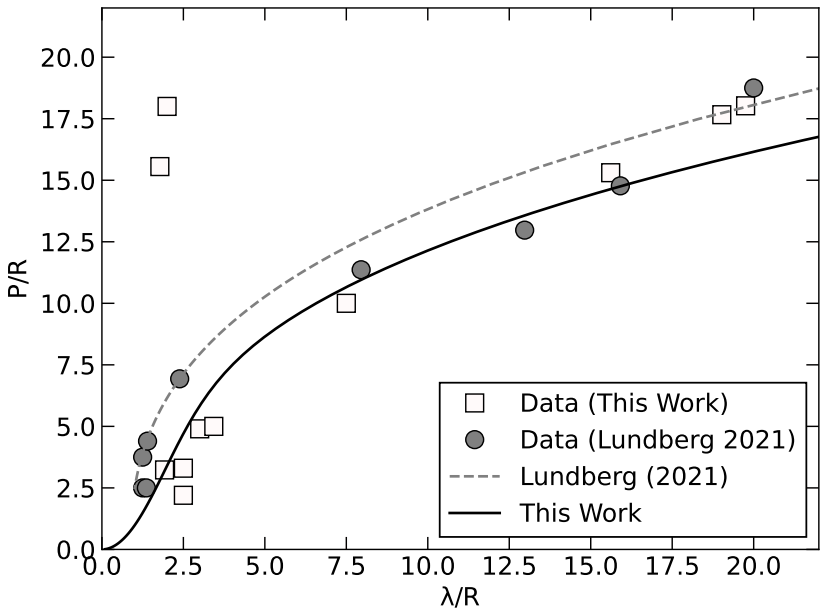

Figure 3.4: Comparison between the theory and data of this work, against the theory and data presented in Lundberg and Strano [25]. The white squares are our interpretation of the literature data, while the grey circles are the interpretation of Lundberg and Strano. Although there is disagreement in the low end, both interpretations agree best with our theory for large λ/R.

side by side in Figure 3.4 with the numerical solution presented in this chapter as the solid black curve, and that of Lundberg and Strano as the dashed grey curve, with the interpretation of the data here represented by the squares, and theirs by the filled circles. They have two extra data points in the small R region, which are excluded from this chapter's data, as no mention of them could be found using the references given in their original paper. For small λ/R, Lundberg and Strano's interpretation agrees better with their results, while the interpretation of the data in this chapter aligns best with the WLC theory. However, both data sets agree best with the WLC results for large λ/R.

3.4 Summary

In this chapter, using the wormlike chain (WLC) polymer model, a numerical solution was produced for the helix pitch P of an infinitely long polymer of persistence length λ wrapped around a nanotube of radius R, using the Green's function approach. It was directly compared to experimental measurements and molecular dynamics simulations for a range of polymers, and was found to accurately predict the observed pitch. Excluded volume effects were not

considered, as monomers in the helix forming polymers are well separated, and experience little overlap. By examining the structure of the theory for large λ/R, the exact scaling behaviour was derived as $P = (2\pi/0.975)(\lambda/R)^{1/3}$ for a polymer wrapped on a small nanotube, which follows the expected Odijk power law that is universal for tightly confined WLC systems.

The results were compared against a different theoretical framework proposed by Lundberg and Strano [25]. It was found that due to differing interpretations of experimental results no conclusions could be drawn for large nanotubes, however both the data in this chapter and Lundberg and Strano's data agreed the best with the WLC theory used for small nanotubes.

The polymers studied in this work were all assumed to have a total contour length much greater than their persistence length ($L \gg \lambda$). Although the considerations of finite length (finite L/λ) are theoretically interesting, and do effect the observed pitch, the effect in this case is small even for $L \approx \lambda$. This puts all the data compared to in this work firmly in the long chain limit, and so it is well modelled by the ground state dominance approach taken here.

Chapter 4

Conclusions

4.1 Summary

The three main chapters of this thesis provided an introduction to the wormlike chain (WLC) polymer theory, numerical methods used to tackle it, and two applications to interesting systems: stretched polymers and helically wrapped carbon nanotubes. The WLC is a common polymer model that accounts for innate polymer stiffness, through a bending energy characterized through the persistence length λ, which is the distance over which tangent vector correlations along the polymer backbone die off. The WLC theory can be analysed using a Green's function approach, which formats the problem in terms of a propagator $q(\mathbf{r}, \mathbf{u}, t)$ which represents the partition function of the polymer with its ends fixed. The propagator in turn can be used to compute global statistical properties through the overall partition function Q, or properties that depend on the monomer positional and orientation distributions, through the density function $\rho(\mathbf{r}, \mathbf{u})$. The propagator itself is the solution to a modified diffusion type equation (MDE) derived from the WLC Hamiltonian.

Although closed form solutions to the MDE for the propagator exist only under certain limits, numerical methods based on discretizing the differential operators over the domain, allow a general solution to be obtained numerically. Here, the Crank-Nicolson method, an average of the backwards and forwards Euler methods, was used to obtain high accuracy numerical solutions. When further accuracy was needed, Richardson extrapolation (see sections 2.2 and 2.3.2) was used to enhance the accuracy of the computations while being more efficient than an equivalent increase in grid points.

Chapter 2 looked at the stretching of polymers with finite length using the WLC model. The treatment of infinitely long chains had been tackled previously, and the approximation was valid due to the long length of the polymer segments used in experiments at that time [2]. Recent experiments have been able to stretch shorter polymer segments, and so a re-examination of the problem that considered finite length effects was needed [40–45]. The average ex-

tension was examined, and an interpolation formula that accurately captured the results, which reduces exactly to the analytic expressions in the high force, low force, and rodlike limits was developed. This formula matched the full set of numerical data to within 1%, and was applicable over the entire parameter space of polymer length and applied forces. This was shown to outperform other finite length theories in the literature, which were either accurate but not applicable over the full parameter space, or applicable everywhere but inaccurate. The mean squared excursion in the direction perpendicular to the applied force was examined, with closed form solutions for rodlike and weak stretching limits presented. This was the first analysis of this parameter for a stretched WLC of finite length in the literature. An interpolation formula was also presented in this case, which captured the numerical results with a maximal error of 6×10^{-4}. The results of this chapter were published in Macromolecules in 2021 [1].

In chapter 3, the WLC was applied to model the helical wrapping of single walled carbon nanotubes by various polymers. Carbon nanotubes are a promising nanomaterial, but solvating and separating them has proven to be a challenging task. Helically wrapping them with different polymers has shown to effectively solvate them, while leaving their interesting electronic properties mostly intact [46–51]. These polymer nanotube systems were modelled as a WLC wrapped around an infinitely long cylindrical surface. Numerically, the helix pitch was computed for a range of nanotube radii. The theoretical framework was also examined to determine the scaling behaviour of the pitch for small nanotubes. Both the scaling and numerical results were found to agree extremely well with experimental measurements for the helix pitch. We compared against another theory, and found that although there was disagreement between the interpretation of the data between this work and theirs, both sets of data agreed best with scaling and numerical data presented here in chapter 3 for small nanotubes. An interpolation formula with a mean squared error of approximately 1.5 in the ratio of helix pitch to nanotube radius was constructed to reproduce the numerical pitch. A draft containing the results from this chapter is being prepared for publication, but is unfinished at the time of writing.

4.2 Outlook

This thesis has shown the application of the common WLC model to two problems, the first was the stretching of finite length polymers in free space, and the second was the helical wrapping of carbon nanotubes by various long polymers. In both cases, the ideal WLC model was used, meaning there was no consideration for any excluded volume interactions, the repulsion of monomers from each other due to the physical space they occupy [89]. Excluded volume is a long range interaction between separated polymer segments, and is difficult to treat theoretically. Under most solvent conditions, it plays an important role in determining the adopted conformation of the polymer. The omission, however, is not striking for the two systems considered. For the shorter polymers modelled for the discussion of finite length stretching, there is little probability

that two monomers with overlap in free space, and so the excluded volume interaction can reasonably be ignored. The same is true for polymers forming a helix around the surface of a nanotube. In a regular helical conformation with a large pitch, as is the adopted conformation, the monomers are well separated from each other and do not interact; excluded volume can safely be ignored in this case as well.

In the case of polymer stretching, the more interesting limit is then the long chain limit, which was originally studied without excluded volume [2]. For a long weakly stretched polymer the chance of overlap is greatly increased, and the excluded volume noticeably swells the chain. This has been demonstrated using Monte Carlo simulations, but no work has been done from the perspective of the WLC [67]. A full WLC treatment, showing the effect of excluded volume, and mapping out its region of importance as a function of polymer length, is then of great interest for future calculations.

There are several points for expansion for the theory of polymer wrapped nanotubes as well. While a full theory was presented for the helix pitch, there are several other metrics of the polymer conformations that are of interest. The first is the confinement free energy. Using the WLC model, it is possible to deduce the free energy scaling in the exact limits of strong and weak confinement, as well as for rodlike and infinitely flexible polymers. Furthermore, the mean squared end-to-end distance both around the nanotube and along it serve as measures of the conformations. These can be calculated using the same type of perturbation theory as was used for the WLC stretching and has been previously used for WLCs in slit confinement [1, 72].

In conclusion, the WLC model has shown itself to be widely applicable, and has been successfully applied to polymer stretching and the wrapping of carbon nanotubes by various polymers. The techniques demonstrated herein can be used to further investigate interesting experimental systems and relevant physical effects that have not yet been considered.

Bibliography

[1] Andersen, N. T.; Teng, Y.; Chen, J. Z. Y. Stretching a Semiflexible Polymer of Finite Length. *Macromolecules* **2022**, *55*, 210–216.

[2] Marko, J. F.; Siggia, E. D. Stretching DNA. *Macromolecules* **1995**, *28*, 8759–8770.

[3] Bouchiat, C.; Wang, M. D.; Allemand, J.-F.; Strick, T.; Block, S. M.; Croquette, V. Estimating the Persistence Length of a Worm-Like Chain Molecule from Force-Extension Measurements. *Biophys. J.* **1999**, *76*, 409–413.

[4] Petrosyan, R. Improved Approximations for Some Polymer Extension Models. *Rheol. Acta* **2017**, *56*, 21–26.

[5] Kessler, D. A.; Rabin, Y. Distribution Functions for Filaments Under Tension. *J. Chem. Phys.* **2004**, *121*, 1155–1164.

[6] Kierfeld, J.; Niamploy, O.; Sa-Yakanit, V.; Lipowsky, R. Stretching of Semiflexible Polymers with Elastic Bonds. *Eur. Phys. J. E* **2004**, *14*, 17–34.

[7] Cathcart, H.; Nicolosi, V.; Hughes, J. M.; Blau, W. J.; Kelly, J. M.; Quinn, S. J.; Coleman, J. N. Ordered DNA Wrapping Switches on Luminescence in Single-walled Nanotube Dispersions. *J. Am. Chem. Soc.* **2008**, *130*, 12734–12744.

[8] Deria, P.; Sinks, L. E.; Park, T.-H.; Tomezsko, D. M.; Brukman, M. J.; Bonnell, D. A.; Therien, M. J. Phase Transfer Catalysts Drive Diverse Organic Solvent Solubility of Single-walled Carbon Nanotubes Helically Wrapped by Ionic, Semiconducting Polymers. *Nano Lett.* **2010**, *10*, 4192–4199.

[9] Yarotski, D. A.; Kilina, S. V.; Talin, A. A.; Tretiak, S.; Prezhdo, O. V.; Balatsky, A. V.; Taylor, A. J. Scanning Tunneling Microscopy of DNA-wrapped Carbon Nanotubes. *Nano Lett.* **2009**, *9*, 12–17.

[10] Kang, Y. K.; Lee, O.-S.; Deria, P.; Kim, S. H.; Park, T.-H.; Bonnell, D. A.; Saven, J. G.; Therien, M. J. Helical Wrapping of Single-Walled Carbon

Nanotubes by Water Soluble Poly (p-phenyleneethynylene). *Nano Lett.* **2009**, *9*, 1414–1418.

[11] Zheng, M.; Jagota, A.; Strano, M. S.; Santos, A. P.; Barone, P.; Chou, S. G.; Diner, B. A.; Dresselhaus, M. S.; Mclean, R. S.; Onoa, G. B., et al. Structure-Based Carbon Nanotube Sorting by Sequence-Dependent DNA Assembly. *Science* **2003**, *302*, 1545–1548.

[12] Campbell, J. F.; Tessmer, I.; Thorp, H. H.; Erie, D. A. Atomic Force Microscopy Studies Of DNA-wrapped Carbon Nanotube Structure and Binding to Quantum Dots. *J. Am. Chem. Soc.* **2008**, *130*, 10648–10655.

[13] Liu, Y.; Chipot, C.; Shao, X.; Cai, W. Free-energy Landscape of the Helical Wrapping of a Carbon Nanotube by a Polysaccharide. *J. Phys. Chem. C* **2011**, *115*, 1851–1856.

[14] Liu, Y.; Chipot, C.; Shao, X.; Cai, W. Solubilizing Carbon Nanotubes Through Noncovalent Functionalization. Insight From the Reversible Wrapping of Alginic Acid Around a Single-Walled Carbon Nanotube. *J. Phys. Chem. B* **2010**, *114*, 5783–5789.

[15] Zerze, G. H.; Stillinger, F. H.; Debenedetti, P. G. The Handedness of DNA Assembly Around Carbon Nanotubes is Determined by the Chirality of DNA. *J. Phys. Chem. B* **2020**, *124*, 5362–5369.

[16] Gurevitch, I.; Srebnik, S. Monte Carlo Simulation of Polymer Wrapping of Nanotubes. *Chem. Phys. Lett.* **2007**, *444*, 96–100.

[17] Chen, H.; Meisburger, S. P.; Pabit, S. A.; Sutton, J. L.; Webb, W. W.; Pollack, L. Ionic Strength-Dependent Persistence Lengths of Single-Stranded RNA and DNA. *PNAS* **2012**, *109*, 799–804.

[18] Murphy, M.; Rasnik, I.; Cheng, W.; Lohman, T. M.; Ha, T. Probing Single-Stranded DNA Conformational Flexibility Using Fluorescence Spectroscopy. *Biophys. J.* **2004**, *86*, 2530–2537.

[19] Morris, G. A.; Castile, J.; Smith, A.; Adams, G. G.; Harding, S. E. Macromolecular Conformation of Chitosan in Dilute Solution: A New Global Hydrodynamic Approach. *Carbohydr. Polym.* **2009**, *76*, 616–621.

[20] Vold, I. M. N.; Kristiansen, K. A.; Christensen, B. E. A Study of the Chain Stiffness and Extension of Alginates, In Vitro Epimerized Alginates, and Periodate-Oxidized Alginates Using Size-Exclusion Chromatography Combined With Light Scattering and Viscosity Detectors. *Biomacromolecules* **2006**, *7*, 2136–2146.

[21] Grell, M.; Bradley, D.; Long, X.; Chamberlain, T.; Inbasekaran, M.; Woo, E.; Soliman, M. Chain Geometry, Solution Aggregation and Enhanced Dichroism in the Liquidcrystalline Conjugated Polymer Poly (9, 9-dioctylfluorene). *Acta Polym.* **1998**, *49*, 439–444.

[22] Fytas, G.; Nothofer, H.; Scherf, U.; Vlassopoulos, D.; Meier, G. Structure and Dynamics of Nondilute Polyfluorene Solutions. *Macromolecules* **2002**, *35*, 481–488.

[23] Jeschke, G.; Sajid, M.; Schulte, M.; Ramezanian, N.; Volkov, A.; Zimmermann, H.; Godt, A. Flexibility of Shape-Persistent Molecular Building Blocks Composed of P-Phenylene and Ethynylene Units. *J. Am. Chem. Soc.* **2010**, *132*, 10107–10117.

[24] Cotts, P. M.; Swager, T. M.; Zhou, Q. Equilibrium Flexibility of a Rigid Linear Conjugated Polymer. *Macromolecules* **1996**, *29*, 7323–7328.

[25] Lundberg, D. J.; Strano, M. S. Approximate Corona Phase Hamiltonian for Individual Cylindrical Nanoparticle–Polymer Interactions. *J. Phys. Chem. B* **2021**,

[26] Brydson, J. A. *Plastics Materials*; Elsevier, 1999.

[27] Staudinger, H. Macromolecular Chemistry. *Nobel Lecture* **1953**, 397–419.

[28] NobelPrize.org, The Nobel Prize in Chemistry 1963. Nobel Prize Outreach AB 2022. https://www.nobelprize.org/prizes/chemistry/1963/summary/, Accessed Thu. 16 Jun 2022.

[29] NobelPrize.org, The Nobel Prize in Chemistry 1974. Nobel Prize Outreach AB 2022. https://www.nobelprize.org/prizes/chemistry/1974/press-release/, Accessed Thu. 16 Jun 2022.

[30] NobelPrize.org, Press Release. Nobel Prize Outreach AB 2022. https://www.nobelprize.org/prizes/physics/1991/press-release/, Accessed Thu. 16 Jun 2022.

[31] Doi, M.; Edwards, S. F. *The Theory of Polymer Dynamics*; Oxford University Press, 1988.

[32] NobelPrize.org, Press Release. Nobel Prize Outreach AB 2022. https://www.nobelprize.org/prizes/chemistry/2000/press-release/, Accessed Mon. 20 Jun 2022.

[33] NobelPrize.org, Press Release. Nobel Prize Outreach AB 2022. https://www.nobelprize.org/prizes/chemistry/2002/press-release/, Accesssed Mon. 20 Jun 2022.

[34] NobelPrize.org, Press Release. Nobel Prize Outreach AB 2022. https://www.nobelprize.org/prizes/chemistry/2005/press-release/, Accesssed Mon. 20 Jun 2022.

[35] Rubinstein, M.; Colby, R. H., et al. *Polymer Physics*; Oxford University Press New York, 2003; Vol. 23.

[36] Metropolis, N.; Ulam, S. The Monte Carlo Method. *J. Am. Stat. Assoc.* **1949**, *44*, 335–341.

[37] Hansson, T.; Oostenbrink, C.; van Gunsteren, W. Molecular Dynamics Simulations. *Curr. Opin. Struct. Biol.* **2002**, *12*, 190–196.

[38] Karplus, M.; Petsko, G. A. Molecular Dynamics Simulations in Biology. *Nature* **1990**, *347*, 631–639.

[39] Kardar, M. *Statistical Physics of Particles*; Cambridge University Press, 2007.

[40] Seol, Y.; Li, J.; Nelson, P. C.; Perkins, T. T.; Betterton, M. D. Elasticity of Short DNA Molecules: Theory and Experiment for Contour Lengths of 0.6–7 μm. *Biophys. J.* **2007**, *93*, 4360–4373.

[41] Sun, Y.-L.; Luo, Z.-P.; An, K.-N. Stretching Short Biopolymers Using Optical Tweezers. *Biochem. Biophys. Res. Commun.* **2001**, *286*, 826–830.

[42] Liu, X.; Pollack, G. H. Mechanics of F-actin Characterized with Microfabricated Cantilevers. *Biophys. J.* **2002**, *83*, 2705–2715.

[43] Chen, Y.-F.; Blab, G. A.; Meiners, J.-C. Stretching Submicron Biomolecules with Constant-Force Axial Optical Tweezers. *Biophys. J.* **2009**, *96*, 4701–4708.

[44] Chen, H.; Fu, H.; Zhu, X.; Cong, P.; Nakamura, F.; Yan, J. Improved High-Force Magnetic Tweezers for Stretching and Refolding of Proteins and Short DNA. *Biophys. J.* **2011**, *100*, 517–523.

[45] Khalil, A. S.; Ferrer, J. M.; Brau, R. R.; Kottmann, S. T.; Noren, C. J.; Lang, M. J.; Belcher, A. M. Single M13 Bacteriophage Tethering and Stretching. *Proc. Natl. Acad. Sci. U.S.A.* **2007**, *104*, 4892–4897.

[46] Zheng, M.; Jagota, A.; Semke, E. D.; Diner, B. A.; McLean, R. S.; Lustig, S. R.; Richardson, R. E.; Tassi, N. G. Dna-Assisted Dispersion and Separation of Carbon Nanotubes. *Nat. Mater.* **2003**, *2*, 338–342.

[47] O'Connell, M. J.; Boul, P.; Ericson, L. M.; Huffman, C.; Wang, Y.; Haroz, E.; Kuper, C.; Tour, J.; Ausman, K. D.; Smalley, R. E. Reversible Water-Solubilization of Single-Walled Carbon Nanotubes by Polymer Wrapping. *Chem. Phys. Lett.* **2001**, *342*, 265–271.

[48] Liu, P. Modifications of Carbon Nanotubes with Polymers. *Eur. Polym. J.* **2005**, *41*, 2693–2703.

[49] Gomulya, W.; Costanzo, G. D.; De Carvalho, E. J. F.; Bisri, S. Z.; Derenskyi, V.; Fritsch, M.; Fröhlich, N.; Allard, S.; Gordiichuk, P.; Herrmann, A., et al. Semiconducting Single-Walled Carbon Nanotubes on Demand by Polymer Wrapping. *Adv. Mater.* **2013**, *25*, 2948–2956.

[50] Star, A.; Stoddart, J. F.; Steuerman, D.; Diehl, M.; Boukai, A.; Wong, E. W.; Yang, X.; Chung, S.-W.; Choi, H.; Heath, J. R. Preparation and Properties of Polymer-Wrapped Single-Walled Carbon Nanotubes. *Angew. Chem.* **2001**, *113*, 1771–1775.

[51] Enyashin, A.; Gemming, S.; Seifert, G. DNA-Wrapped Carbon Nanotubes. *Nanotechnology* **2007**, *18*, 245702.

[52] Chen, J. Z. Theory of Wormlike Polymer Chains in Confinement. *Prog. Polym. Sci.* **2016**, *54*, 3–46.

[53] Saitô, N.; Takahashi, K.; Yunoki, Y. The Statistical Mechanical Theory of Stiff Chains. *J. Phys. Soc. Jpn.* **1967**, *22*, 219–226.

[54] Kratky, O.; Porod, G. Röntgenuntersuchung Gelöster Fadenmoleküle. *Recl. Trav. Chim. Pays-Bas* **1949**, *68*, 1106–1122.

[55] Odijk, T. Theory of Lyotropic Polymer Liquid Crystals. *Macromolecules* **1986**, *19*, 2313–2329.

[56] Thomas, J. W. *Numerical Partial Differential Equations: Finite Difference Methods*; Springer Science & Business Media, 2013; Vol. 22.

[57] Quarteroni, A.; Sacco, R.; Saleri, F. *Numerical Mathematics*; Springer Science & Business Media, 2010; Vol. 37.

[58] Birkhoff, G.; Rota, G.-C. *Ordinary Differential Equations*; John Wiley & Sons, Ltd, 1989; p 211.

[59] Richardson, L. F.; Gaunt, J. A. Viii. The Deferred Approach to the Limit. *Philos. Trans. R. Soc. A* **1927**, *226*, 299–361.

[60] Richardson, L. F.; Glazebrook, R. T. Ix. The Approximate Arithmetical Solution by Finite Differences of Physical Problems Involving Differential Equations, with an Application to the Stresses in a Masonry Dam. *Philos. Trans. R. Soc. A* **1911**, *210*, 307–357.

[61] Smith, S. B.; Finzi, L.; Bustamante, C. Direct Mechanical Measurements of the Elasticity of Single DNA Molecules by Using Magnetic Beads. *Science* **1992**, *258*, 1122–1126.

[62] Schurr, J. M.; Smith, S. B. Theory for the Extension of a Linear Polyelectrolyte Attached at One End in an Electric Field. *Biopolymers* **1990**, *29*, 1161–1165.

[63] Perkins, T. T.; Smith, D. E.; Larson, R. G.; Chu, S. Stretching of a Single Tethered Polymer in a Uniform Flow. *Science* **1995**, *268*, 83–87.

[64] Livadaru, L.; Netz, R. R.; Kreuzer, H. J. Stretching Response of Discrete Semiflexible Polymers. *Macromolecules* **2003**, *36*, 3732–3744.

[65] Hori, Y.; Prasad, A.; Kondev, J. Stretching Short Biopolymers by Fields and Forces. *Phys. Rev. E* **2007**, *75*, 041904.

[66] Benetatos, P.; Terentjev, E. M. Stretching Weakly Bending Filaments with Spontaneous Curvature in Two Dimensions. *Phys. Rev. E* **2010**, *81*, 031802.

[67] Li, X.; Schroeder, C. M.; Dorfman, K. D. Modeling the Stretching of Wormlike Chains in the Presence of Excluded Volume. *Soft Matter* **2015**, *11*, 5947–5954.

[68] Kurzthaler, C. Elastic Behavior of a Semiflexible Polymer in 3D Subject to Compression and Stretching Forces. *Soft Matter* **2018**, *14*, 7634–7644.

[69] Feynman, R. P. *Statistical Mechanics: A Set Of Lectures*; Westview Press, 1998.

[70] Crank, J.; Nicolson, P. A Practical Method for Numerical Evaluation of Solutions of Partial Differential Equations of the Heat-Conduction Type. *Proc. Camb. Phil. Soc.* **1947**, *43*, 50–67.

[71] https://github.com/ntsmande/SASPOFL-Numerical-Data.git.

[72] Teng, Y.; Andersen, N. T.; Chen, J. Z. Y. Statistical Properties of a Slit-Confined Wormlike Chain of Finite Length. *Macromolecules* **2021**, *54*, 8008–8023.

[73] Keller, D.; Swigon, D.; Bustamante, C. Relating Single-Molecule Measurements to Thermodynamics. *Biophys. J.* **2003**, *84*, 733–738.

[74] Benetatos, P.; Razbin, M. Orientational Fluctuations and Bimodality in Semiflexible Nunchucks. *Polymers* **2021**, *13*.

[75] Samanta, S. K.; Fritsch, M.; Scherf, U.; Gomulya, W.; Bisri, S. Z.; Loi, M. A. Conjugated Polymer-Assisted Dispersion of Single-Wall Carbon Nanotubes: The Power of Polymer Wrapping. *Acc. Chem. Res.* **2014**, *47*, 2446–2456.

[76] Chik, M. W.; Hussain, Z.; Zulkefeli, M.; Tripathy, M.; Kumar, S.; Majeed, A. B. A.; Byrappa, K. Polymer-Wrapped Single-Walled Carbon Nanotubes: A Transformation Toward Better Applications in Healthcare. *Drug Deliv. Transl. Res.* **2019**, *9*, 578–594.

[77] Li, Y.; Li, G.; Wang, X.; Zhu, Z.; Ma, H.; Zhang, T.; Jin, J. Poly (Ionic Liquid)-Wrapped Single-Walled Carbon Nanotubes for Sub-Ppb Detection of CO2. *Chem. Commun.* **2012**, *48*, 8222–8224.

[78] Gomulya, W.; Gao, J.; Loi, M. A. Conjugated Polymer-Wrapped Carbon Nanotubes: Physical Properties and Device Applications. *Eur. Phys. J. B* **2013**, *86*, 1–13.

[79] Li, Z.; Song, Y.; Li, A.; Xu, W.; Zhang, W. Direct Observation of the Wrapping/Unwrapping of ssDNA Around/From a SWNT at the Single-Molecule Level: Towards Tuning the Binding Mode and Strength. *Nanoscale* **2018**, *10*, 18586–18596.

[80] Johnson, R. R.; Johnson, A. C.; Klein, M. L. Probing the Structure Of DNA- Carbon Nanotube Hybrids with Molecular Dynamics. *Nano Lett.* **2008**, *8*, 69–75.

[81] Tallury, S. S.; Pasquinelli, M. A. Molecular Dynamics Simulations of Flexible Polymer Chains Wrapping Single-Walled Carbon Nanotubes. *J. Phys. Chem. B* **2010**, *114*, 4122–4129.

[82] Arkin, H.; Janke, W. Polymer Adsorption on Curved Surfaces. *Phys. Rev. E* **2017**, *96*, 062504.

[83] Gurevitch, I.; Srebnik, S. Conformational Behavior of Polymers Adsorbed on Nanotubes. *J. Chem. Phys.* **2008**, *128*, 144901.

[84] Kumar, S.; Pattanayek, S. K.; Pereira, G. G. Organization of Polymer Chains Onto Long, Single-Wall Carbon Nano-Tubes: Effect of Tube Diameter and Cooling Method. *J. Chem. Phys.* **2014**, *140*, 024904.

[85] Chen, J. Z. Free Energy and Extension of a Wormlike Chain in Tube Confinement. *Macromolecules* **2013**, *46*, 9837–9844.

[86] Liang, Q.; Li, J.; Zhang, P.; Chen, J. Z. Y. Modified Diffusion Equation for the Wormlike-Chain Statistics in Curvilinear Coordinates. *J. Chem. Phys.* **2013**, *138*, 244910.

[87] Hagerman, P. J. Flexibility of DNA. *Annu. Rev. Biophys.* **1988**, *17*, 265–286.

[88] Odijk, T. The Statistics and Dynamics of Confined or Entangled Stiff Polymers. *Macromolecules* **1983**, *16*, 1340–1344.

[89] Flory, P. J. *Principles of Polymer Chemistry*; Cornell university press, 1953.

[90] Grosberg, A. Y.; Khokhlov, A. R. *Statistical Physics of Macromolecules*; American Inst. of Physics, 1994.

[91] Harris, C. R. et al. Array Programming with NumPy. *Nature* **2020**, *585*, 357–362.

[92] Virtanen, P. et al. SciPy 1.0: Fundamental Algorithms for Scientific Computing in Python. *Nat. Methods* **2020**, *17*, 261–272.

Appendices

Appendix A

Ground State Dominance (GSD)

A.1 GSD Theory

The goal behind the ground state dominance (GSD) theory is to develop a method to calculate the long chain limit $L \to \infty$ (keeping λ fixed) of the system of interest. This theoretical limit applies to polymers whose length is much larger than their persistence length, mathematically $L/\lambda \gg 1$. It is not uncommon to find real experimental polymers that are well approximated under this limit, and so the GSD method finds use in a number of applications [90].

The starting point is the wormlike chain (WLC) modified diffusion equation (MDE), equation 1.17

$$\frac{\partial}{\partial t} q(\mathbf{r}, \mathbf{u}, t) = \left[-L\mathbf{u} \cdot \nabla_{\mathbf{r}} \big|_{\mathbf{u}} + \frac{L}{2\lambda} \nabla^2_{\mathbf{u}} - U[\mathbf{r}, \mathbf{u}] \right] q(\mathbf{r}, \mathbf{u}, t)$$

The idea is to expand the propagator $q(\mathbf{r}, \mathbf{u}, t)$ in terms of the eigenstates ψ of the operator on the right-hand side of the equation, denoted A

$$A = \left[-L\mathbf{u} \cdot \nabla_{\mathbf{r}} \big|_{\mathbf{u}} + \frac{L}{2\lambda} \nabla^2_{\mathbf{u}} - U[\mathbf{r}, \mathbf{u}] \right] \tag{A.1}$$

where μ is the dimensionless free energy per unit length. The eigenvalue equation is

$$A\psi_n = -\mu_n L \psi_n \tag{A.2}$$

The eigenstates of the propagator are assumed to have the variable separated form

$$\psi_n(\mathbf{r}, \mathbf{u}, t) = e^{-\mu_n L t} \psi_n(\mathbf{r}, \mathbf{u}) \tag{A.3}$$

and so the expansion of $q(\mathbf{r}, \mathbf{u}, t)$ then has the general form

$$q(\mathbf{r}, \mathbf{u}, t) = \sum_n C_n e^{-\mu_n L t} \psi_n(\mathbf{r}, \mathbf{u}) \tag{A.4}$$

where C_n are the expansion coefficients. In taking the limit $L \to \infty$, the sum becomes dominated by the term with the lowest energy μ, corresponding to the ground state. For the long chain limit then, it is sufficient to compute the smallest eigenvalue μ, and its associated eigenvector $\psi_{\min}$. This gives

$$q(\mathbf{r}, \mathbf{u}, t) = C_n e^{-\mu_{\min} L t} \psi_{\min}(\mathbf{r}, \mathbf{u}) \tag{A.5}$$

As discussed in section 1.4, the partition function is related to the integral of the propagator

$$Q = \int q(\mathbf{r}, \mathbf{u}, t = 1) \, \mathrm{d}\mathbf{r}\mathrm{d}\mathbf{u} \tag{A.6}$$

Under GSD, this then becomes

$$Q = \int C_n e^{-\mu_{\min} L} \psi_{\min}(\mathbf{r}, \mathbf{u}) \, \mathrm{d}\mathbf{r}\mathrm{d}\mathbf{u} \tag{A.7}$$

As the integral over $\psi_{\min}(\mathbf{r}, \mathbf{u})$ is a constant, B, the partition function then has the form

$$Q = D e^{-\mu_{\min} L} \tag{A.8}$$

If one is working in the canonical / Helmholtz ensemble, then the Helmholtz free energy is readily obtained from the partition function

$$\beta F = -\ln Q \tag{A.9}$$

where $\beta = 1/k_b T$ is the inverse of the product of the Boltzmann constant times the temperature. Substituting in the GSD partition function directly yields

$$\beta F = \mu L - \ln D \approx \mu L \tag{A.10}$$

for $L \to \infty$. Hence, computing μ directly gives the energy (Helmholtz free energy, or Gibbs free energy, depending on the problem). The eigenstate $\psi_{\min}$ can be used to compute the density distribution ρ_{GSD} following the same reasoning (see section 1.4) and its associated long chain results, as is done throughout chapter 3.

A.2 GSD Numerical Implementation

The exact implementation of the diagonalization scheme of the operator A can vary. Marko and Siggia solved the polymer stretching problem for $L \to \infty$ by expanding $q(\theta)$ in terms of spherical harmonics analytically, then solving the resulting matrix equation up to degree $l = 100$ numerically for the smallest eigenvalue [2]. This approach was reproduced in chapter 2 to produce the GSD limit in figure 2.3 (a).

For the GSD results in figure 2.3 (b) and in chapter 3, the operator A is numerically discretized, using a central difference scheme (see section 1.5.1). The resulting smallest eigenvalue and associated eigenvector are then solved for numerically, using the NumPy Python library, which in turn uses the optimized BLAS and LAPACK linear algebra libraries [91]. In chapter 3, the GSD matrix was implemented as a sparse matrix, with 3×10^6 non-zero elements, using the SciPy Python library [92].

Appendix B

Exact Strong Stretching Calculation

Here, the calculation of the exact strong stretching results for $\langle z \rangle$ and $\langle R_{xy}^2 \rangle$, as presented in chapter 2, are shown. The Hamiltonian for a stretched WLC is given by

$$\beta H = \int_0^1 \mathrm{d}t \left[\frac{\lambda}{2L} \left| \frac{\mathrm{d}\mathbf{u}(t)}{\mathrm{d}t} \right|^2 - \beta L f u_z(t) \right]$$

Under high force, the tangent vector u_z deviates only slightly from the stretching direction z, and so it can be expanded to quadratic order in terms of the tangent vector in the xy plane u_{xy} to give $u_z \approx 1 - u_{xy}^2/2$, and so the strongly stretched WLC Hamiltonian becomes

$$\beta H = \int_0^1 \mathrm{d}t \left[\frac{\lambda}{2L} \left| \frac{\mathrm{d}\mathbf{u}(t)}{\mathrm{d}t} \right|^2 + \frac{1}{2} \beta L f u_{xy}^2(t) \right] - \beta L f \tag{B.1}$$

This approximation to the tangent vector fluctuations at high force is the basis for all the high force results used by the studies discussed in chapter 2, for both long and short chains.

A Hamiltonian of this type is similar to that for a quantum harmonic oscillator, and mapping to such a problem allows the use of existing solutions for the propagators in quantum mechanics to be applied to the WLC. Using the result from Feynman for the two point greens function of a quantum harmonic oscillator [69]

$$G(\mathbf{u}_{xy}, \mathbf{u}'_{xy}, \tau) = A e^{-B(\mathbf{u}_{xy}^2 + \mathbf{u}_{xy}'^2) + 2\pi A \mathbf{u}_{xy} \cdot \mathbf{u}'_{xy}} \tag{B.2}$$

where the terminal ends are separated by a fractional length $\tau = t - t'$, and the value of the perpendicular vectors at the points are $\mathbf{u}_{xy}$ and $\mathbf{u}'_{xy}$ respectively.

The A, B functions are

$$A = \frac{\alpha}{2\pi} \frac{1}{\sinh \gamma\tau} \tag{B.3}$$

$$B = \pi A \cosh \gamma\tau \tag{B.4}$$

and the associated coefficients are $\alpha = (\lambda\beta f)^{1/2}$ and $\gamma = L(\beta f/\lambda)^{1/2}$. Integrating the Green's function over all values of $\mathbf{u}_{xy}$ and $\mathbf{u}'_{xy}$ gives the partition function

$$\frac{Q}{V} = \frac{2\pi}{\alpha \sinh \gamma} \tag{B.5}$$

which can then be used to calculated the Gibbs free energy, and associated extension

$$\frac{\langle z \rangle}{L} = 1 - \frac{1}{\beta f L} D\left(L\sqrt{\frac{\beta f}{\lambda}}\right) \quad \text{(for } \tilde{f} \gg 1 \text{ and any } \tilde{L}\text{)} \tag{B.6}$$

with

$$D(x) = \left[1 + x \coth\left(x\right)\right]/2 \tag{B.7}$$

as was presented in the main text.

A similar procedure is taken in order to calculate the strong stretching limit of $\langle R_{xy}^2 \rangle$. First, one looks at the orientational correlation function for the two monomers at t and t', which is obtained from the product of the three Green's functions $G(\mathbf{u}_0, \mathbf{u}, \mathbf{u}', \mathbf{u}_1, t) \equiv G(\mathbf{u}_0, \mathbf{u}, t)G(\mathbf{u}, \mathbf{u}', t-t')G(\mathbf{u}', \mathbf{u}_1, 1-t')$, where all the $\mathbf{u}$ vectors are confined to the xy plane. Each component Green's function here represents a segment of the polymer connected to the two monomers (terminal to monomer 1, monomer 1 to 2, and monomer 2 to terminal). Integrating, one obtains the two point correlation function

$$\langle \mathbf{u} \cdot \mathbf{u}' \rangle = \frac{2\cosh(\gamma t)\cosh(\gamma[1-t'])}{\alpha \sinh(\gamma)} \quad \text{for } t' \geq t \tag{B.8}$$

Performing an integral over the correlation function for all t, t', then gives the projection of the mean squared end-to-end distance in the xy plane.

$$\langle R_{xy}^2 \rangle = L^2 \int_0^1 \int_0^1 \langle \mathbf{u} \cdot \mathbf{u}' \rangle \, \mathrm{d}t' \mathrm{d}t = \frac{2L}{\beta f} \tag{B.9}$$

which although simple is applicable to any chain length $\tilde{L}$ for large forces $\tilde{f} \gg 1$.

Appendix C

Polymer Wrapped SWNT: Literature Data and Lundberg Theory

This appendix contains two items supporting the discussion presented on polymer wrapped single walled carbon nanotubes (SWNTs) in chapter 3. The first is the implicit equation for the helix pitch presented by Lundberg and Strano, and how the results from their theory were reproduced in this work. The second is the list of experimental data points (10 unique studies spanning 6 different polymer systems) used to compare to our numerical theory in chapter 3, and how they were adapted from their respective papers. A separate analysis of the literature for an independent quotation of the same studies used for comparison in the work of Lundberg and Strano was necessary, as their table presenting the data points and how they were obtained was unclear [25].

C.1 Comparison Against Lundberg and Strano

For the comparison against the theory by Lundberg and Strano, their interpretation of the experimental data was taken directly as presented in their SI, without any modifications [25]. Their theory, given as the dashed grey curve in Figure 4 in the main text, was obtained by solving their eq. (23). Using the notation in this work, the equation is

$$-2\lambda\frac{R^2P/2\pi}{(R^2+(P/2\pi)^2)^{3/2}}+F(\alpha)\left[\frac{1}{\sqrt{R^2+(P/2\pi)^2}}-\left(\frac{(P/2\pi)^2}{(R^2+(P/2\pi)^2)^{3/2}}\right)\right]=0 \tag{C.1}$$

Where $F(\alpha)$ is

$$F(\alpha)=\frac{k_BT}{\lambda}\left(\alpha-\frac{1}{4}+\frac{1}{4(1-\alpha)^2}-\frac{3}{4}\alpha^2\right) \tag{C.2}$$

and $\alpha = (P/2\pi)/\sqrt{R^2 + (P/2\pi)^2}$.

For each data point, R was fixed, and the value of $P/2\pi$ that satisfies the equation was numerically solved for via a root finding algorithm, as implemented in the SciPy numerical library [92]. The resulting curve exactly matches the numerical curve presented by Lundberg and Strano in their Figure 2.

C.2 Literature Data

The experimental data values for the helix pitch of single walled carbon nanotubes (SWNTs) wrapped by various polymers as presented in Figure 2 in the main text are given here. Values of for the helix pitch were taken directly from the papers of interest. If the paper gave a value of for the persistence length λ of the system, it was used. If no value for λ was given, it was estimated using separate experimental studies, with the specific value selected to properly account for the ionic strength of the experimental / theoretical system. See the table below for details on what papers were used. The cylinder radius used in our model was taken as the radius of the SWNT, plus the distance from the surface of the nanotube to the polymer backbone, and is referred to as the hybrid radius. This is given in tabulated form in Table C.1 below. All values for the hybrid radius were taken directly as reported in their papers, save for two papers which did not report a nanotube radius. These exceptions and how the nanotube radius was estimated are noted in the table on the next page. The table lists if the paper is experimental or theoretical, with the theoretical further divided into Monte Carlo (MC) and Molecular Dynamics (MD) simulations.

Table C.1: Experimental data points, estimated persistence length, and nanotube radii

Authors	Exp / Sim	System	λ (nm)	P (nm)	R (nm)
Cathcard 2008 [7]	Exp	2x ssDNA	2.5 [17, 18]	2.2	1
Liu 2011 [13]	Sim (MD)	Chitosan	16 ± 2 [19]	14.6 ± 1.7	0.81
Liu 2010 [14]	Sim(MD)	Alginic Acid	15.3 ± 0.5 [20]	15*	0.98
Deria 2010 [8]	Exp	PNES[d]	7.5 [21, 22]	10 ± 2	1
Yarotski 2009 [9]	Exp + Sim (MD)	ssDNA	2.5 [17, 18]	3.3 ± 0.2 ; 4.2**	1 ; 1.3[a]
Kang 2009 [10]	Exp + Sim (MD)	PPES[d]	14 [23, 24]	13 ± 2	0.736
Zheng 2003 [11]	Exp	ssDNA	2 [17, 18]	18	1[b]
Campbell 2008 [12]	Exp	ssDNA	1.6 [17, 18]	14 ± 5	0.9
Zerze 2020 [15]	Sim (MD)	ssDNA	3 [17, 18]	4.9 ± 0.7	1
Gurevitch 2008 [83]	Sim (MC)	Generic[c]	10.3σ [16]	15σ	3σ

* Estimated based off Figure 1.
** Semicolon separates experimental data from simulation data (Experimental ; Theory)
a Taken from Figure 4 [9]
b Assuming that the ssDNA backbone is ~ 0.5 nm above the surface, as done by Campbell et al. for the same $(GT)_{30}$ polymer [12]
c A general parameter σ was used in the work instead of specific values
d PNES and PPES are abbreviations of chemical names for molecules without common names. See the List of Abbreviations for the full definitions.